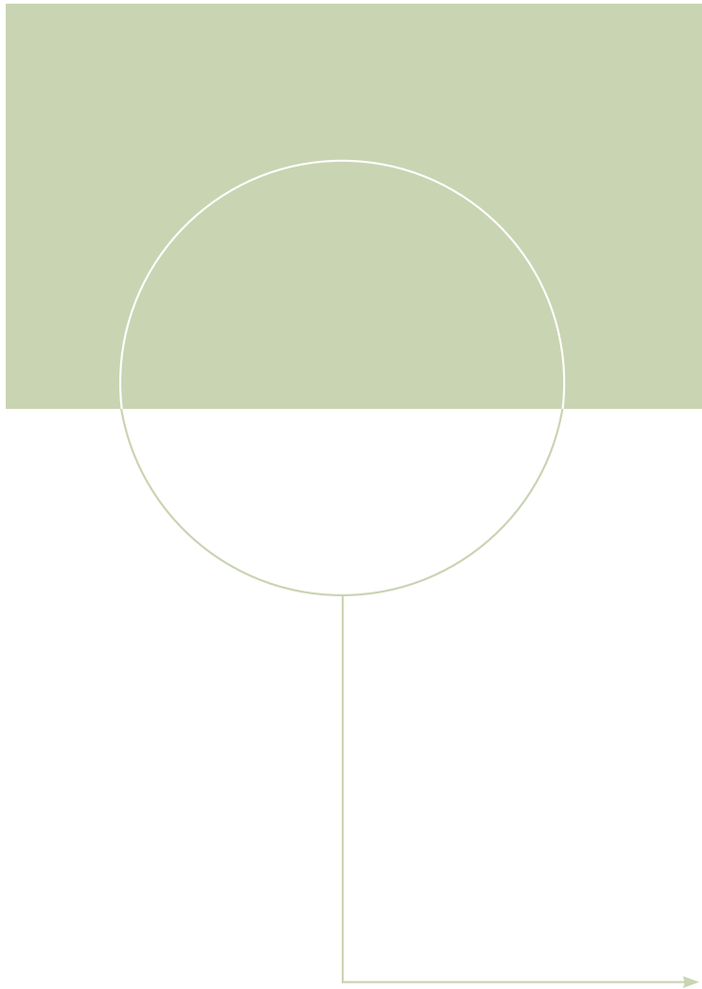

Master's thesis

2019

Andreas Rise Mathisen

NTNU
Norwegian University of
Science and Technology
Faculty of Information Technology and Electrical
Engineering
Department of Electric Power Engineering

Master's thesis

Andreas Rise Mathisen

Continuous-Time Unit Commitment using spline interpolation

June 2019

NTNU
Norwegian University of
Science and Technology

NTNU
Norwegian University of
Science and Technology

NTNU

Norwegian University of
Science and Technology

Continuous-Time Unit Commitment using spline interpolation

Andreas Rise Mathisen

Energy and Environmental Engineering
Submission date: June 2019
Supervisor: Hossein Farahmand

Norwegian University of Science and Technology
Department of Electric Power Engineering

Preface

This Master's Thesis is written at the Department of Electric Power Engineering at the Norwegian University of Science and Technology (NTNU) during the spring of 2019 and concludes my Master of Science (MSc) degree in Energy and Environmental Engineering. The thesis focuses on fundamental concepts related to power system operation and optimization and is written under the supervision of Associate Professor Hossein Farahmand at the Department of Electric Power Engineering, NTNU.

Working with this thesis has given me a unique insight into power system operation and optimization, and it has given me insight into challenges related to current and future power systems. The thesis has provided me with an excellent foundation for future work within the topic, but I also hope that the work and results in this thesis will inspire others to dig further into the topic.

Acknowledgment

First of all, I would like to thank my supervisor Associate Professor Hossein Farahmand and my co-supervisor Postdoctoral Fellow Jamshid Aghaei for letting me work with such an interesting topic. Being privileged enough to work with what interests me the most has truly motivated me to work with this thesis and has stimulated my interest to work with this topic also after this MSc has been submitted.

I want to extend my deepest gratitude to Hossein for his guidance throughout the project. Although he has a busy schedule, he's found time for meetings to give valuable input and feedback on my work. This has truly been invaluable. I would also like to thank Ph.D. Candidate Christian Øyn Naversen at the Department of Electric Power Engineering for his input on robust optimization. His input has given me a better understanding of robust optimization, and has been essential for the robust optimization formulation designed in this thesis.

Andreas Rise Mathisen

Abstract

Power system operators are facing increasing challenges with both scheduling and real-time (RT) operation of generating units. The day-ahead unit commitment (UC) is a well-established and essential part of today's power system operation, where forecast load data is used to schedule the next-day commitment and operation of generating units. A well-formulated UC problem formulation, where ramping and generating constraints are incorporated is crucial to ensure an effective power system operation. This translates down to both economic and stability aspects, where the aim is both to reduce operating costs as well as ensuring sufficient ramping and generating reserves are available in the power system at all times.

The current day-ahead UC problem models load forecasts as constant in hour-intervals, where load change between hours is modeled as step functions. There are several reasons why this formulation is so well-established and widely used. It is simple and effective. However, it has some major weaknesses. It is effective when load forecasts are accurate and when sub-hourly variations in load are low. In power systems with high penetration of variable renewable energy sources (VRES), two main problems are: 1) Power output from VRES is highly intermittent and hard to predict accurately, and 2) large and steep variations in power output from VRES require large ramping reserves. The current day-ahead UC formulation does not capture such sub-hourly variations and sharp ramping events, which can lead to ramping scarcity during RT operation of power systems.

In this thesis, a continuous time day-ahead UC problem formulation will be considered by using spline interpolation. The model uses the very same day-ahead load data as the current UC model but will use this data not only to schedule generating output profiles but also ramping profiles. Hence, sub-hourly variations will be considered and generating units will be incorporated into the UC problem. Furthermore, two modifications will be assessed and applied to

this UC model are namely to 1) formulate robust generating constraints and 2) introduce energy storage (ES) units in the system. The proposed UC model is formulated as a mixed integer linear programming (MILP) problem and will be compared to the traditional UC problem through simulations based on historical load data.

Simulations are based on load data from California ISO (CASIO), and show that overall, the proposed Bernstein UC model outperforms the traditional UC model in terms of both operating costs and scarcity events. The models perform similarly when day-ahead load forecasts are accurate, but for load data with large forecast errors, steep ramping and large sub-hourly load variations, the Bernstein model performs significantly better. RT operation costs are kept much lower with the Bernstein model, much because the traditional model relies more heavily on auxiliary generation during RT operation due to ramping and generating scarcity.

In the cases where ES units were introduced, it became clear that robust operating constraints were beneficial to keep sufficient generating and ramping capacity available in the system during the charging/discharging cycles of the ES units. The Bernstein model and the traditional model performed close to equally well when identical robust constraints were applied to both models, however, the natural robust nature of the Bernstein UC model ensured the model performed excellently also without added robust generating constraints. That was not the case for the traditional UC model.

Sammendrag

Nåværende kraftsystemer står overfor økende utfordringer knyttet til både planleggings og sanntidsdrift av generatorenheter. Dagen-før Unit Commitment (UC) er en veletablert og viktig del av dages kraftsystemdrift, der prognoselastdata brukes til å planlegge driftstatus of produksjonseffekt fra generatorenheter. En velformulert UC-problemformulering hvor ramping og generasjonskapasitet tas høyde for er avgjørende for å sikte effektiv drift av kraftsystemer. Dette kan oversettes både ned til økonomi- og stabilitetsaspekter, hvor målet er både å minimere driftskostnader såvel som å sikre a tilstrekkelige rampe- og generasjonsreserver er tilgjengelige i kraftnettet til enhver tid.

Den nåværende UC-problemmodellen modellerer lastprognoser som konstante på timesintervaller, hvor lastendringen mellom timesintervaller er modellert som stegfunksjoner. Der er flere grunner til at denne formuleringen er så veletabler og mye brukt; den er enkel og den er effektiv. Den har likevel enkelte klare svakheter. Den er effektiv når lastprognosene er nøyaktige og når lastvariasjonene innad i timesintervallene er små. I kraftsystemer med en høy gpenetrasjon av variable fornybare energikilder (VRES) er to hovedproblemer at: 1) kraftproduksjon fra VRES er svært avhengig av værmønster og vanskelig å forutse nøyaktig, og 2) store og skarpe variasjoner i utgangseffekt fra VRES krever store rampe-reserver. Den nåværende dagen-før UC-formuleringen fanger ikke ikke opp variasjoner innad i timesintervaller and skarpe rampehendelser, noe som kan føre til rampeknapphet under sanntidsdrift av kraftsystemer.

I denne oppgaven blir en kontinuerlig dagen-før UC problemformulering presentert ved å bruke Bernstein-polynomer av grad 3. Modellen benytter nøyaktig de samme dagen-før lastdatasettene som dagens model, men den vil bruke disse dataene ikke bare til å definere kraftproduksjonsgrenser, men også rampegrenser. Dermed vil variasjoner inad i timersintervaller fanges opp slik at drift av generatorenheter planlegges også på grunnlag av rampeegenskaper. Videre vil to modifikasjoner vurderes og anvendt på denne modellen, 1) formulere ro-

buste produksjonsgrenser for generatorene i systemet og 2) innføre energilagrings (ES)-enheter i systemet. Modellen formuleres som en Mixed Integer Linear Programming (MILP) problem og sammenlignes med sin motpart UC-formulering med timesvis konstante lastprognoser, for hver simulering.

Simuleringene er basert på lastdata fra California ISO, og viser at totalt sett, så presterer den foreslåtte Bernstein UC-modellen bedre enn den tradisjonelle UC-modellen, både når det gjelder driftskostnader og knapphetshendelser. Modellene presterer begge akseptabelt når dage-før lastprognosene er nøyaktige, men for lastdatene med store prognosefeil presterer Bernstein-modellen betydelig bedre enn den tradosjonelle modellen. Sanntids driftskostnader holdes generelt mye lavere med Bernstein-modellen, mye grunnet at den tradisjonelle modellen avhenger i langt større grad av kraft fra hjelpe-generatorer under sanntidsdrift på grunn av knapphet på generasjonskapasitet og ramping.

I tilfellene hvor ES-enherter ble introdusert i kraftsystemet, kom det tydelig fram at robuste driftsbetingelser var fordelsaktige for å sørge for at tilstrekkelig renererings- og rampekapasitet var tilgjengelig under lade- og utladningssyklusene til ES-enhetene. Bernstein-modellen og den tradisjonelle modellen presterte nært like bra når identiske robuste genereringsgrenser ble brukt på begge modeller, men Bernstein-modellen presterte langt bedre enn den tradisjonelle modellen uten robuste grensebetingeler.

Contents

List of Figures

List of Tables

Abbreviations

ES	Energy Storage
RT	Real-time
UC	Unit Commitment
VRES	Variable Renewable Energy Source
MILP	Mixed Integer Linear Programming
ISO	Independent System Operator
IEEE RTS	IEEE Reliability Test System
DA	Day-ahead
SOC	State of Charge

Nomenclature

g, e, v, d, l	generating unit, ES unit, VRES unit,load bus and transmission line index
$H(.), B(.)$	Hermite spline and Bernstein polynomial index
k	integer hour interval index
$\mathbf{D}(t)$	load demand vector
$\mathbf{G}(t)$	power generating vector
$\mathbf{E}(t)$	state of charge vector
$N(t)$	net load demand
$P(t)$	power flow variable
$R(t)$	ramping variable
$U(t, g)$	Generating unit commitment variable
$Y(t, g)$	Generating unit startup variable
$Z(t, g)$	Generating unit shutdown variable
η_c	charging efficiency

η_d	discharging efficiency
$P_{max,min}$	maximum/minimum power flow
SU	maximum startup ramping
SD	maximum shutdown ramping
C_{SU}	Startup costs
C_{SD}	Shutdown costs
RU, RD	maximum ramp up and ramp down rate rate
UT	minimum up-time
DT	minimum down-time
U_{ini}	initial commitment status for generating unit
U_0	initial ontime
S_0	initial offtime
CU	Upward reserve marginal cost
CD	Downward reserve marginal cost
E_{max}	Maximum storage capacity
E_{ini}	Initial energy level
C_{DA}	DA UC scheduling costs
C_{RT}	RT operation costs
C_{NET}	Net UC costs
$c_{(.)}$	RT cost function

$\Delta G_g^{+/-}(t)$	Up-/ down spinning reserves
ω_L, ω_U	lower/upper boundaries of confidence interval
$\Delta N_{R,(.)}^{k,(.)}$	robust uncertainty set at time interval k

Chapter 1

Introduction

1.1 Motivation

The UC problem is a key aspect of power system operation and involves determining start-up and shut down schedules of thermal generating units, as well as the deployment of ES resources, to meet a forecasted load in a future short-term period[2]. Power system operation planning process is a continuous-time mixed integer problem[3] that is commonly broken into discrete time steps as an approximation. Reducing the continuous-time time frame to a given set of time intervals enables the use of a finite set of variables to determine operation schedules.

The UC problem consists of several markets, including several RT-markets and forward markets, of which the day-ahead market is where most of the bulk-energy trading takes place. The day-ahead UC problem where generating units are scheduled day-ahead in 24-periods is well established. An independent system operator (ISO) operates energy markets and is responsible for scheduling and committing generators based on generating offers and load forecasts[4]. As explained, the current day-ahead UC problem formulation models day-ahead forecasted loads as piecewise constant on hour-intervals and solves the UC problem as an optimization problem the most economically with an array of constraints into taken consideration.

In recent years, there has been a steady increase in installed wind capacity worldwide, with 51.3 GW being installed in 2018[5]. This is a part of the transition from thermal energy generation to renewable energy generation. With

an ever-increasing world population and electrification, the increase in installed VRES is a natural trend that will continue for the foreseeable future. This development is also accelerated by the Paris Agreement[6] that emphasizes that global greenhouse gas emissions have to be reduced to keep global temperature rise this century below the critical 2 degrees Celsius goal. VRES such as wind turbines and photovoltaics are expected to play a crucial role in this development, as they produce close to emission-free and renewable power and provide unique opportunities for future power supply. Their variable nature, however, introduces major challenges to power system operations.

Power systems with a high penetration of VRES can experience significant ramping stress and scarcity, as VRES output is challenging to forecast and integrate into power system operations on a large scale. The current day-ahead UC with hourly constant generating schedules is designed for and works well for power systems with low variability, but it's starting to fall inadequate for power systems with a high penetration of VRES. The motivation for this thesis will thus be to test the use of a continuous-time formulation of the UC problem that reflects intra-hour load variations and better account for ramping constraints and profiles.

1.2 Scope

The continuous time UC formulation proposed in this thesis (denoted Bernstein UC model) is based on Hermite spline data interpolation and Bernstein polynomials. The traditional day-ahead UC formulation uses load forecasts in hour intervals to determine the next day UC schedule. The proposed Bernstein UC model will be based on the same exact input data as the traditional UC model.

The Bernstein UC model will use the DA forecast load data to estimate the ramping of the next day load trajectory, and use this as an input parameter for the day-ahead UC problem. A combination of the properties of Hermite splines and Bernstein polynomials will be used to schedule smooth and continuous generating curves, that also satisfy ramping and generating capacity constraints in the system.

In addition to the Bernstein UC problem formulation, 4 sub-models will be defined and tested to assess the impact of a set of possible future power system scenarios. These models are designed to highlight the impact of 1) having ISO operated ES units available in the power system, and 2) robust spinning reserve constraints. The 4 different sub-models are:

- Standard UC model

- Robust UC model
- Standard UC model with ES units
- Robust UC model with ES units

To compare the Bernstein model with the traditional UC model, the UC problem will be simulated on historical load data. The simulations will determine DA operating costs and calculate the RT economic dispatch based on RT load data. This thesis will only consider the day-ahead UC schedule and do not include the effects of the hour-ahead energy market or the 5-minute RT energy market. The goal for the Bernstein UC formulation is to reduce forecasting and scheduling errors in the day-ahead UC model and to better capture sub-hourly load variations. Hence, it is justifiable to exclude the hour-ahead and RT energy market from the model. Demand response is also not considered in this thesis.

1.3 Contributions

This thesis aims at developing an alternative day-ahead UC model that better approximates load ramping and thus reduces scheduling errors of day-ahead UC, compared to the current UC model. The continuous-time UC formulation will be designed to better capture sub-hourly load variations as well as the intermittent generating nature of VRES.

The proposed UC model uses the same load forecasts as the current UC model, but schedules the operation of thermal and ES units through Hermite spline coefficients, instead of a step function. Hence, it can be considered as a modification or simply an extension of the current UC model, that schedules thermal and ES units based also on forecasted ramping trajectories such that online units can respond more efficiently to load variations during RT operation.

1.4 Structure

Chapter 1 - *Introduction*, provides the main background and concepts for the thesis, and defines scope and structure of the thesis.

Chapter 2 - *Unit Commitment*, explains main concepts related to UC scheduling and proposes a Bernstein UC problem model.

Chapter 3 - *Test System*, provides a detailed overview of the IEEE 24-Bus Reliability Test System(RTS), UC model definitions, and UC sub-models.

Chapter 4 - *Robust Optimization*, introduces fundamental robust optimization concepts and presents the robust UC model that will be used in this thesis.

Chapter 5 - *Case Studies*, lists the load data cases that will be simulated in this thesis.

Chapter 6 - *Discussion*, lists results from the case studies, and discusses and interprets the results.

Chapter 7 - *Conclusion*, draws conclusions from Chapter 5 and presents suggestions for future work.

Chapter 2

Unit Commitment

2.1 Background

The day-ahead UC problem has a pivotal role in power system operation, and likewise, optimization techniques to solve the UC problem are constantly being developed and improved. Extensive optimization literature surveys are discussed in [7][8][9]. The UC problem is very commonly formulated as a MILP problem, with a given set of floating variables and binary variables determining commitment. A high number of binary variables yield high computational costs, so it is typically an aim to keep the number of binary variables to a minimum. In [10], the UC problem is solved using only a single binary variable. For transparency, this thesis will use a MILP UC formulation with 3 binary variables, respectively representing startup, shutdown and commitment status.

One of the major weaknesses of the current day-ahead UC problem formulation is that it does not directly capture sub-hourly variations in load. This can yield high marginal prices during RT operation, resulting in a sub-optimal RT economical dispatch for both the ISO as well as load consumers. The issue can be improved by applying a "brute force" method of simply reducing the step size of the UC scheduling intervals. Although this approach improves the accuracy of the traditional UC model, it has some clear limitations. 1) Narrowing the step size of the scheduling interval increases the number of UC scheduling variables exponentially. 2) Discrete approximations do not reflect the continuous-time ramping of the load. 3) Increasing the number for scheduling intervals would also require more load forecast data and could potentially

complicate the day-ahead energy bidding and trading process[11].

2.2 Previous attempt on improving UC scheduling accuracy

A number of UC models have been designed, aiming to better incorporate ramping constraints in the day-ahead generating unit scheduling. In [12][13] and [14], ramping constraints are integrated into the UC problem though nonlinear dynamic programming. The papers model ramping as linear on discrete-time intervals on a finite number of time steps. The authors in [15] use interior point methods to solve the UC problem as a composite of linear discrete time problems bounded together by ramping constraints. In papers [16][17][18] and [19], ramping is incorporated into the UC problem as a discrete-time MILP problem solved by Lagrangian relaxation, modeling ramping as piecewise constant on discrete time intervals.

Dynamic programming has a tendency of being computationally exhaustive, and all of the UC models referenced in the above paragraph solves the UC problem as piecewise linear on discrete time intervals instead of a continuous-time formulation. The authors in [20] and [3] solves the UC problem as a continuous-time UC problem formulation operating with decision variables in one-hour intervals, similar to the approach proposed in this thesis.

To account for day-ahead load forecasting errors, it is also common to include security constraints in the form of spinning and/or standing reserve requirements. Two security constrained UC formulations are presented in [21][22], and both models use spinning reserve constraints. While security constrained UC models often result in higher DA scheduling costs, they may yield lower RT operation costs and net UC costs than a standard UC formulation. Appropriate security constraints must be selected wisely for optimal effect. This will be addressed in Chapter 4. But while security constraints can improve UC problem RT operation costs, their impact may only be so good in the current UC problem formulation, as sub-hourly load variations are not captured in the UC scheduling.

For the proposed Bernstein UC model, it is desirable to maintain the hourly scheduling profile of generating units. The Bernstein UC model will be using the same hourly binary variables as the traditional UC model, but instead of one variable describing the constant hourly power profile, four Hermite spline coefficient variables will be used, and they can yield an infinite number of load

and generation trajectories while also imposing continuity and smoothness.

2.3 General UC operation Constraints

The UC problem is an optimization problem subject to a number of constraints, including generating unit and ES unit power limits, ramping constraints, and thermal limits for transmission lines. The balancing constraint for the UC problem is that generating input must be equal to the power demand in the system. In cases of extreme generating capacity scarcity it may be necessary with load shedding, and similarly in cases with a large overproduction from VRES, wind or solar curtailment may be necessary[23]. These means, and load shedding, in particular, may be extremely expensive and should be kept to a minimum.

At any given time, to maintain power system stability, the power generated must be equal power consumed by loads. An advantage with a continuous time UC problem formulation is that there also is an emphasis on power ramping trajectories. By also considering these trajectories, the number of ramping scarcity events in the grid could be reduced compared to the traditional day-ahead UC formulation that only schedules for constant power balance on hourly intervals.

$$\sum_{e,v,g} G(t) - \sum_{v} G_{curtail}(t) = \sum_{d} D(t) + \sum_{e} D(t) - \sum_{d} D_{shred}(t) \tag{2.1}$$

$$\sum_{e,v,g} R(t) = \sum_{d} R(t) \tag{2.2}$$

Equation 2.1 represents a general power balance, while 2.2 describes the ramping trajectory balance between loads and generating units. The operation and scheduling of generating units and ES units is based on cost functions, power and ramping capacities, as well as available reserves.

2.3.1 Generating and ES unit constraints

There are a number of constraints that restrict how generating and ES units can be operated, given by the physical properties of the respective units. These constraints described in the section below. Certain operation constraints are dependent on the commitment status of thermal units in the power system. These binary variables are described below.

2.3.2 Binary operational variables

The day-ahead UC problem in this thesis is formulated on a per-hour basis, meaning that start-ups, shutdowns, and commitment status are considered in hourly intervals. Let the variable $U(t, g)$ denote commitment status for generating unit g at time t, $Y(t, g)$ denotes a start-up, and the variable $Z(t, g)$ denotes a shutdown sequence. These variables are used for both the traditional UC model and the proposed Bernstein UC model, but their interpretation is slightly different for the two models. Let the figure below illustrate:

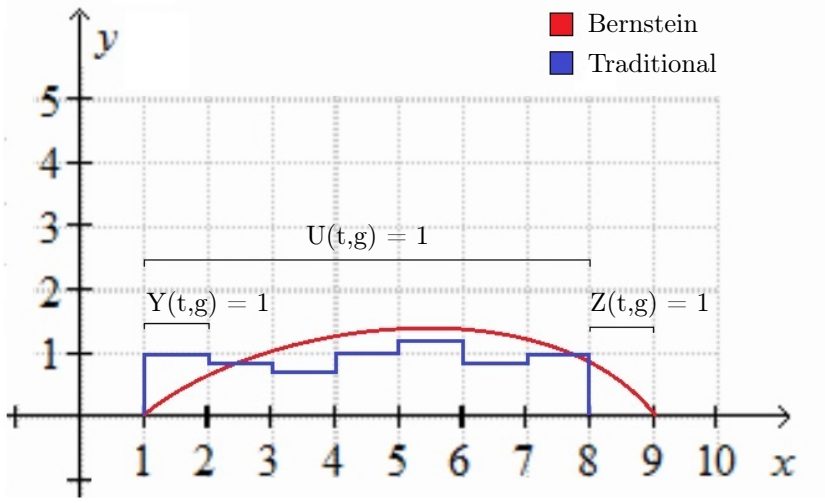

Figure 2.1: Binary UC variables

As seen in Figure 2.1, the Bernstein generating curve is continuous, and for this UC formulation, the variables $Y(t, g)$ and $Z(t, g)$ initiate startup- and shutdown intervals. I.e., the generating profile is at nominal operation at the end of the time interval for these variables. For the traditional UC formulation, there is no continuity requirement, and for the startup- and shutdown intervals, the nominal operation is assumed from the start of the interval. For both formulations, there is an overlap between the variable $Y(t, g) = 1$ and $U(t, g) = 1$. Due to the slightly different binary variable interpretations for the two UC models, their operating constraints are correspondingly implemented differently. The constraints are formulated below.

Bernstein model

$$(U(t,g) - Y(t,g))P_g^{min} \leq P_g(t) \leq (U(t,g) + Z(t,g))P_g^{max} \tag{2.3}$$

Traditional model model

$$U(t,g)P_g^{min} \leq P_g(t) \leq U(t,g)P_g^{max} \tag{2.4}$$

Equation 2.3 and Equation 2.4 define lower and upper bounds for the power output from generating units. Notice that the power output from the thermal units is restricted by the commitment status of the respective units. This is because thermal units have minimum up- and downtimes and cannot instantly be started up or shut down.

Power and energy constraints

$$P_{e,v,l}^{min} \leq P_{e,v,l}(t) \leq P_{e,v,l}^{max} \tag{2.5}$$

$$D_{e,d}^{min} \leq D_{e,d}(t) \leq D_{e,d}^{max} \tag{2.6}$$

Equation 2.5 is similar to Equation 2.4, and applies to VRES, ES units and transmission lines. VRES and ES units do not have commitment variables, and their operation is hence not bounded to certain periods of the day. The lower bounds for the ES units define the maximum charging power, while upper bounds define maximum discharging power. The power constraints for transmission lines is given by thermal limits, and in many cases, $P_l^{min} = -P_l^{max}$, as power can flow bidirectionally. In other cases, e.g. when power flows through a transformer, the power may be restricted to flowing unidirectionally, such that $P_l^{min} = 0$. Equation 2.6 describes the minimum and maximum loading limits of the system. These constraints limit the charging/discharging cycles of the ES units in the system.

$$E_e^{min} \leq E_e(t) \leq E_e^{max} \tag{2.7}$$

In Equation 2.7, the term E_e^{max} describes the maximum energy storage capacities of the ES units, while E_e^{min} describes the minimum stored energy. While the upper bounds only reflect the maximum storage capacity of the units, the lower bounds are very much dependent on the type of ES system, as certain ES systems suffer from accelerated degradation at a low state of charge (SOC)[24][25]. ES systems like e.g. lithium-ion batteries can experience significant degradation with deep discharge cycles, while e.g. hydrogen fuel cells are

not heavily affected by deep discharging. The stored energy in an ES unit at time **t** is given as:

$$E(t) = E(t_0) + \int_t (\eta_c D(\tau)_e - \frac{G(\tau)_e}{\eta_d}) d\tau \tag{2.8}$$

In the energy balance in 2.8, η_c and η_d respectively represent the charging and discharging efficiencies of the ES unit. An important note, however, is that the daily self-discharge is neglected in the energy balance equation. This is a valid assumption for 1) short energy storage durations, and 2) for ES systems with low self-discharge losses. The term $E(t_0)$ represents the initial energy in an ES unit at the beginning of the UC scheduling interval.

Ramping constraints

In addition to power and energy constraints, all generating and ES units in power systems have ramping constraints. The thermal units have different generating constraints for startup, nominal operation and shutdown, as has been discussed in [20]. The constraints can be written as:

$$\frac{dP_g(t)}{dt} \leq SU_g Y(t,g) + RU_g(U(t,g) - Y(t,g) + Z(t,g)) \tag{2.9}$$

$$\frac{dP_g(t)}{dt} \geq -RD_g U(t,g) - SD_g Z(t,g) \tag{2.10}$$

$$-RD_e \leq \frac{dP_e(t)}{dt} \leq RU_e \tag{2.11}$$

The constraint above ensure that a thermal or ES unit cannot instantly change its power output (or input). Equations 2.9 and 2.10 define these constraints as a function of the binary variables $U(t,g)$, $Y(t,g)$ and $Z(t,g)$, and SU(maximum startup ramp), RU(maximum ramp), RD(maximum ramp down) and SD(maximum shutdown ramp). For this thesis it will be assumed that the same ramping limits apply to both charging and discharging of ES units, which is expressed in Equation 2.11.

2.3.3 Convention

For convenience, the load demand, power output, ramping, ES energy state and thermal unit commitment status, can be represented in vectors denoted by the

bold-faced letters $\mathbf{D}(t) = [D(t)_1, ..., D(t)_n]^T$, $\mathbf{G}(t) = [G(t)_1, ..., G(t)_n]^T$, $\mathbf{R}(t) = \frac{d\mathbf{P}(t)}{dt} = [R(t)_1, ..., R(t)_n]^T$, $\mathbf{E}(t) = [E(t)_1, ..., E(t)_n]^T$ and $\mathbf{U}(t) = [U(t)_1, ..., U(t)_n]^T$. The dimensions of these vectors are a function of number of load buses, thermal, ERES and ES units.

While generating units, VRES units and demand buses have a uni-directional flow of power, ES units have a bi-directional power flow. This means that an ES can operate in two different states, namely charging, or discharging state (stationary can be classified as either of these two states). During charging, the ES unit will be seen as a load from the grid, and it will be seen as a generating unit during discharging. As the generating units g only operate in one state, they can be represented with only g commitment variables, $U(t,g)$. The e ES units can operate in two states, and for simplicity, the following definitions are made:

$$G_e(t) = \begin{cases} P_e(t), & \text{if} P_e(t) \geq 0 \\ 0, & \text{otherwise} \end{cases} \tag{2.12}$$

$$D_e(t) = \begin{cases} -P_e(t), & \text{if} P_e(t) \leq 0 \\ 0, & \text{otherwise} \end{cases} \tag{2.13}$$

During charging, the ES units absorb energy from the grid and can be considered as a positive load, and during discharging they deliver power to the grid and can be considered as a generating unit. This is expressed in Equations 2.12 and 2.13, where each ES unit is described by one load- and one generating unit variable. The dimension of the vectors described above are as follows:

$$dim\mathbf{D}(t) = d + e \tag{2.14}$$

$$dim\mathbf{G}(t) = g + v + e \tag{2.15}$$

$$dim\mathbf{R}(t) = g + 2e + v + d \tag{2.16}$$

$$dim\mathbf{U}(t) = g \tag{2.17}$$

$$dim\mathbf{E}(t) = e \tag{2.18}$$

The dimension of $\mathbf{D}(t)$ in 2.14 is given by the number of system units that consume power. The dimension of $\mathbf{G}(t)$ in 2.15 is given by the number of system

units that deliver power to the grid. The dimension of $\mathbf{R}(t)$ in 2.16 is given by the ramp rates of all system units. The ES units have one ramp-rate describing charging and one ramp-rate describing discharging (they are assumed to be equal in this thesis). As shown in Equation 2.17, the generating units have one commitment variable each. Equation 2.18 describes the energy content in the ES units in the system and thus $\mathbf{E}(t)$ has the dimension e.

2.4 UC objective function

The day-ahead UC problem is solved based on load demands, subject to all constraints listed in Section 2.3. The UC problem itself is an optimization problem that can be solved based on a number of different objective functions. Some different UC environments include *Cost based UC*, *Price based UC*, *Profit based US* and *Security based US*. In [9], these UC objective models are described as:

- *Cost based UC* - the objective is to minimize production costs. Satisfying hourly loads is a restriction.
- *Price based UC* - on/off statuses of generating units are decided by fuel purchase prices and energy sales prices. Satisfying hourly loads is not a restriction.
- *Profit based UC* - the objective is to maximize profit. Satisfying hourly loads is not a restriction.
- *Security based UC* - the objective is to minimize production costs, given added security constraints. Satisfying hourly loads is a restriction.

This thesis will consider *Cost based UC* and *Security based UC* models. They have identical objective functions, and the *Security based UC* models used will be derived as an extension of the *Cost based UC* models, with added spinning reserve constraints. The objective functions are described below.

2.4.1 Cost Based objective function

The net operation costs for the UC commitment problem is a sum of the DA UC scheduling costs and RT operational costs. The DA UC problem will be

solved based on the DA objective cost function, but the overall performance of the UC model also depends on RT costs. The DA objective function is:

$$C_{DA} = \sum_{g} \int_{t=0}^{t_{end}} (c_g(U_g(t,g), G_g(t)) + SU_g \epsilon_g^{SU}(t) + SD_g \epsilon_g^{SD}(t))dt + \sum_{e} \int_{t=0}^{t_{end}} (c_{e,d}(G_e(t)) - c_{e,c}(D_e(t)))dt + \sum_{d} \int_{t=0}^{t_{end}} (c_{shred}(D_{shred}(t)))dt \tag{2.19}$$

In 2.19, $c_g(U_g(t,g), G_g(t))$ represents the generation costs [\$/MWh] of generation unit g at time t as a function of commitment power output. $\epsilon_g^{SU,SD}$ represent infinitely small logical functions that initiate start-up and shutdown-costs. $c_{e,d}(G_e(t))$ and $c_{e,c}(D_e(t))$ respectively represent discharging and charging costs for ES units, while $c_{shred}(D_{shred}(t))$ represents load shredding costs. Assuming that adequate generating capacity is available to meet all loads, no load shredding is allowed in DA planning of the *Cost Based UC* model. In the DA cost function, costs of VRES generation is assumed to be negligible. The DA UC problem is solved by minimizing the objective function, Equation 2.19.

The RT operation cost function is similar to the DA cost function but is calculated in RT. In a perfect load and VRES forecast and scheduling scenario, RT operation costs are equal to zero. Hence, RT operation costs reflect how effective a given day-ahead UC model formulation is, as poor and inaccurate scheduling results in high RT costs. The RT cost function is:

$$C_{RT} = \sum_{g} \int_{t=0}^{t_{end}} (CU_g(\Delta G_g^{+}(t)) + CD_g(\Delta G_g^{-}(t)))dt + \sum_{aux} \int_{t=0}^{t_{end}} (c_{aux}(G_{aux}(t)))dt + \sum_{d} \int_{t=0}^{t_{end}} (c_{shred}(\Delta D_{shred}(t)))dt + \sum_{v} \int_{t=0}^{t_{end}} (c_{curtail}(\Delta G_{curtail}(t)))dt \tag{2.20}$$

In Equation 2.20, $CU_g(\Delta G_g^{+}(t))$ and $CD_g(\Delta G_g^{-}(t))$ respectively represent the cost of applying up- and down reserves of the committed generating units. $c_{aux}(G_{aux}(t))$ represents the cost of auxiliary generation that is committed to supply extra ramping or generating capacity in the system in RT. The last two terms in the equation represent the cost of unscheduled load shedding and VRES curtailment.

While minimizing Equation 2.19 will be the objective function for the DA scheduling problem, the performance of the UC model will be evaluated in terms of how well the sum of Equation 2.19 and 2.20 has been minimized. The cost C_{DA} is calculated before the scheduling period, while D_{RT} is known only at the end of the scheduling period. This can be expressed as:

$$C_{NET} = \min(C_{DA} + C_{RT}) \tag{2.21}$$

The net operational costs explained in Equation 2.21 will be used as one of the indicators to assess and compare the performance of the proposed Bernstein UC model with the traditional UC model in this thesis.

2.5 The traditional day-ahead UC model implementation

The UC model uses one floating variable, describing the magnitude of the power output[10]. The same goes for scheduling of ES unit operation. The magnitude of the power output and input is obviously bounded by the maximum and minimum power and energy capacities of the thermal and ES units. The ramping capacities are considered from hour to hour:

$$P(k)_{g,e} - P(k-1)_{g,e} \leq (U(k-1,g) - Y(k-1,g) + Z(k-1,g))RU_{g,e} + Y(k-1,g)SU_{g,e} \tag{2.22}$$

$$P(k)_{g,e} - P(k-1)_{g,e} \geq -U(k-1,g)RD_{g,e} - Z(k-1,g)SD_{g,e} \tag{2.23}$$

Equation 2.22 and 2.23 constrain the maximum and minimum ramping of units from hour $k-1$ to k. The ramping limits are only considered as average ramping per hour.

2.5.1 UC model vairables

The traditional UC model has 3 logical variables per thermal unit, and 1 variable denoting the magnitude of hourly power flow. The ES units have 3 variables per hourly interval, one denoting charging, one denoting discharging and one for ES state of charge.

2.6 The Bernstein day-ahead UC model

A goal for the proposed continuous time UC formulation is to base the US model on the same available input data as for the traditional UC model, and it is desirable to use this data to estimate the ramping of the load at these hour interval points. For a continuous-time UC formulation, the hour to hour ramping constraints used for the traditional UC model (Equation 2.22 and Equation 2.23) are no longer sufficient, as they do not capture or constrain intra-hour ramping variations. These issues will be addressed in this section.

2.6.1 Estimating DA load ramping

The forecasted net system load at time interval k is denoted $N(k)$, and the forecasted ramping at the same points as $R(k)$. The ramping $R(k)$ can be approximated numerically by using a finite difference method. Using the numerical approximation method described [26], the point ramping can be approximated as:

$$R(k)_{end} = \frac{-3N(k) + 4N(k+1) - N(k+2)}{2k} \tag{2.24}$$

$$R(k)_{mid} = \frac{N(k+1) - N(k-1)}{2k} \tag{2.25}$$

The three-point approximation method in 2.24 will be used to approximate the ramping in endpoints, while the two-point approximation in 2.25 will be used to approximate ramping in midpoints.

2.6.2 Hermite Splines

Now that the ramping and magnitude of the load is estimated at each hour-interval point, it is desirable to establish a continuous time function that interpolates all the values into one load forecast curve. *Hermite spline interpolation* is a powerful tool that is widely employed to smoothly interpolate a curve between data points[27]. This is illustrated in the figure below.

In Figure 2.2, the points $N(k)$ and $N(k+1)$ correspond to the magnitude of the forecasted load at times k and $k+1$, while $R(k)$ and $R(k+1)$ correspond with the ramping of the curve of the same points. The smooth curve between the points is obtained simply by multiplying the 4 load forecast points with 4 Hermite basis polynomials and add them together[27]. The four polynomials are:

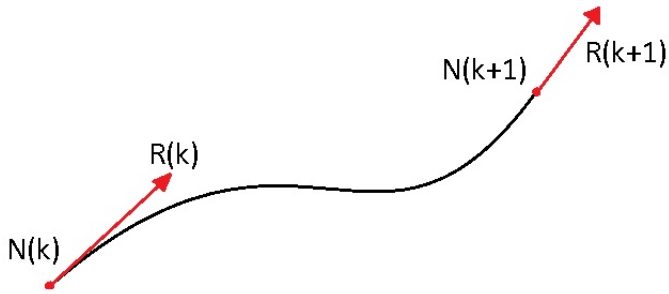

Figure 2.2: Hermite Spline Interpolation

$$H_{00}(t) = 2t^3 - 3t^2 + 1 \tag{2.26}$$
$$H_{01}(t) = t^3 - 2t^2 + t \tag{2.27}$$
$$H_{10}(t) = -2t^3 + 3t^2 \tag{2.28}$$
$$H_{11}(t) = t^3 - t^2 \tag{2.29}$$

The polynomials in 2.26 can be used to create a continuous time curve inside time intervals. Between each time interval k and k, the time variable t ranges linearly from $t = 0$ to $t = 1$. Notice that for $t = 0$, $H_{00}(t) = 1$ while all other polynomials are zero, and for $t = 1$, $H_{10}(t) = 1$ while all other polynomials are zero. There will be one continuous time curve for each time interval k. For convenience, one can introduce the coefficients $N^k_{H00} = N(k)$, $N^k_{H01} = R(k)$, $N^k_{H10} = N(k+1)$ and $N^k_{H11} = R(k+1)$. The continuous time curve can then be expressed as:

$$N_H(k,t) = N_{H00}(k)H_{00}(t) + N_{H01}(k)H_{01}(t) + N_{H10}(k)H_{10}(t) + N_{H11}(k)H_{11}(t) \tag{2.30}$$

Equation 2.30 describes the interpolated load curve for time interval k, with the continuous time subinterval $t \in [0, 1]$ for each k. For $k = k_{end}$, it is assumed that $N(k+1) = N(k)$. A key property automatically implied from the Hermite spline interpolation, is continuity and smoothness between time intervals. The time interval coefficients are related as follows:

$$N_{H10}(k) = N_{H00}(k+1) \tag{2.31}$$

$$N_{H11}(k) = N_{H01}(k+1) \tag{2.32}$$

Equation 2.31 relates the magnitude of the load curve at the end of a period k to the magnitude of the curve at the beginning of the next period $k + 1$. Similarly, Equation 2.32 relates the ramping between intervals. This means for each time interval, the load forecast for the Bernstein UC model is composed of 4 coefficients, as opposed to 1 for the traditional UC formulation. Analogous to this, the thermal and ES will be scheduled with 4 coefficients for each interval.

Generating and ES unit trajectory

With the load forecasts modeled by Hermite splines, it follows naturally to also model ES and generating unit trajectories by the same approach. For this, one can use a similar denotation as for the load forecast curve. Let generating curves and load curves be denoted as:

$$G_H^{g,e}(k,t) = G_{H00}^{g,e}(k)H_{00}(t) + G_{H01}^{g,e}(k)H_{01}(t) + G_{H10}^{g,e}(k)H_{10}(t) + G_{H11}^{g,e}(k)H_{11}(t) \tag{2.33}$$

$$D_H^{d,e}(k,t) = D_{H00}^{d,e}(k)H_{00}(t) + D_{H01}^{d,e}(k)H_{01}(t) + D_{H10}^{d,e}(k)H_{10}(t) + D_{H11}^{d,e}(k)H_{11}(t) \tag{2.34}$$

Equation 2.33 describes the thermal unit output and ES unit discharging curves, while Equation 2.34 describes ES unit charge trajectories as well as load forecasts at load bus d. Please note that $N_H(k,t) = \sum_d D_H^d(k,t)$. While smoothness is implicitly implied for the load forecast model, it is not for the generating trajectories, as generating trajectories can be considered independent for each time interval k. To enforce continuity, it is hence necessary to define constraints that relate the generating trajectories. These constraints are similar to Equation 2.31 and Equation 2.32.

$$G_{H10}^{g,e}(k) = G_{H00}^{g,e}(k+1) \tag{2.35}$$
$$G_{H11}^{g,e}(k) = G_{H01}^{g,e}(k+1) \tag{2.36}$$
$$D_{H10}^{e}(k) = D_{H00}^{e}(k+1) \tag{2.37}$$
$$D_{H11}^{e}(k) = D_{H01}^{e}(k+1) \tag{2.38}$$

The constraints 2.35 enforce magnitude continuity and ramping continuity in the intersection points of the time intervals. However, these constraints alone are not enough to enforce generating capacity and ramping constraints for generating trajectories. While the coefficients in 2.35 can be used to constrain ramping and power output at the hourly interval intersection points, they do not directly constrain intra-hour variations. To enforce this, a linear change of basis to Bernstein polynomials will be used.

2.6.3 Bernstein polynomials

There are several spline models that can be used to approximate the continuous trajectory curve of an interpolation problem, based on a set of discrete data sets. The order of these splines will increase the accuracy of the trajectory model. Like the Hermite splines, Bernstein polynomials are a widely employed interpolation tool, with its most powerful feature being the convex hull property. This will be addressed later in this section. A Bernstein polynomial is defined by:

$$B_{i,n}(t) = \binom{n}{i} t^i (1-t)^{n-1} \tag{2.39}$$

In 2.39, $\binom{n}{i}$ represents the binomial coefficient, and the Bernstein polynomials of degree n form the basis for the power polynomials of degree n[28]. A linear combination of these polynomials can be used to create an infinite number of trajectory curves. The Hermite polynomial in 2.30 can be linearly transformed to a Bernstein power polynomial of degree 3 through a change of basis matrix.

Figure 2.3 shows the Bernstein polynomials of degree 3, as well as the trajectory curve of each respective polynomial. As for the Hermite spline, a linear combination of these polynomials can be used to determine generating and ES power flow trajectories. For this, the Bernstein coefficients $G^{g,e}_{Bi3}(k)$ and $D^{d,e}_{Bi3}(k)$ are introduced, and the power trajectories can be expressed as:

$$G^{g,e}_{B}(k,t) = G^{g,e}_{B03}(k)B_{0,3}(t) + G^{g,e}_{B13}(k)B_{1,3}(t) + G^{g,e}_{B23}(k)B_{2,3}(t) + G^{g,e}_{B33}(k)B_{3,3}(t) \tag{2.40}$$

$$D^{d,e}_{B}(k,t) = D^{d,e}_{B03}(k)B_{0,3}(t) + D^{d,e}_{B13}(k)B_{1,3}(t) + D^{d,e}_{B23}(k)B_{2,3}(t) + D^{d,e}_{B33}(k)B_{3,3}(t) \tag{2.41}$$

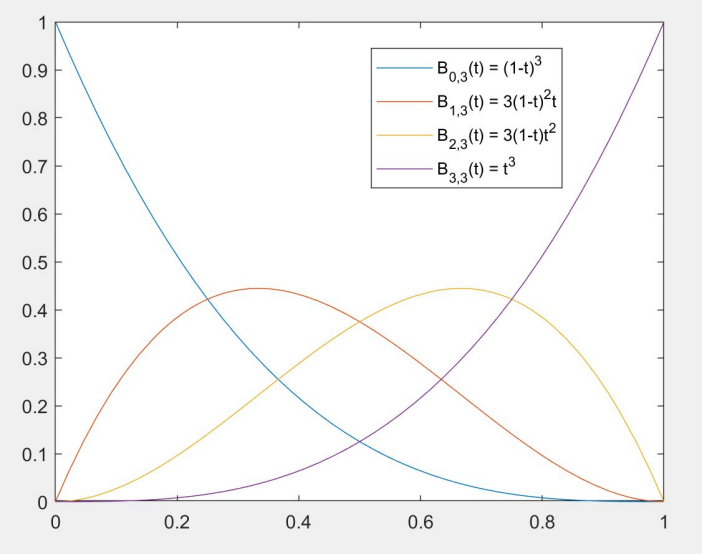

Figure 2.3: Bernstein polynomials of degree 3

Equation 2.40 and Equation 2.41 are power flow curves on the same form as 2.33 and Equation 2.34. As Hermite splines and Bernstein polynomials of degree 3 are linearly related, it is possible relate the Bernstein and Hermite polynomials as follows $G_H^{g,e}(k,t) = G_B^{g,e}(k,t)$, $D_H^{d,e}(k,t) = D_B^{d,e}(k,t)$. This approach has beed used in [3] and [20], and yields the following:

$$\mathbf{H}(t) = \mathbf{D}\mathbf{B}_3(t) \rightarrow \mathbf{G}_H^{g,e}(k) = \mathbf{D}^T\mathbf{G}_{B3}^{g,e}(k) \tag{2.42}$$

where $\mathbf{D}$ is the change-of-basis matrix

$$D = \begin{bmatrix} 1 & 1 & 0 & 0 \\ 0 & \frac{1}{3} & 0 & 0 \\ 0 & 0 & 1 & 1 \\ 0 & 0 & -\frac{1}{3} & 0 \end{bmatrix} \tag{2.43}$$

In 2.43, the vectors $\mathbf{H}(t) = [H_{00}(t), H_{01}(t), H_{10}(t), H_{11}(t)]^T$ and $\mathbf{B}_3(t) = [B_{03}(t),$
$B_{13}(t), B_{23}(t), B_{33}(t)]^T$ are related through the matrix $\mathbf{D}$, and subsequently the coefficient vectors $\mathbf{G}_H^{g,e}(k) = [G_{H00}^{g,e}(k), G_{H01}^{g,e}(k), G_{H10}^{g,e}(k), G_{H11}^{g,e}(k)]^T$ and

$\mathbf{G}_{B3}^{g,e}(k) = [G_{B03}^{g,e}(k), G_{B13}^{g,e}(k), G_{B23}^{g,e}(k), G_{B33}^{g,e}(k)]^T$ are related through the transpose of the matrix $\mathbf{D}$.

Ramping trajectory

The generating curve $G_B^{g,e}(k,t)$ describes the power flow to/from thermal and ES units, and hence the slope of the curve, or ramping, is given by the derivative of this function. Any Bernstein power polynomial of degree *(n-1)* can be written as a linear combination of Bernstein polynomials of degree n[29]. Hence it is possible to write the derivative of a degree 3 Bernstein power polynomial as a linear combination of Bernstein polynomial of degree 2. This has been done in [3]:

$$\dot{\mathbf{B}}_3(t) = \mathbf{A}\mathbf{B}_2(t) \tag{2.44}$$

where $\mathbf{A}$ is the matrix

$$A = \begin{bmatrix} -3 & 0 & 0 \\ 3 & -3 & 0 \\ 0 & 3 & -3 \\ 0 & 0 & 3 \end{bmatrix} \tag{2.45}$$

In Equation 2.44, $\mathbf{B}_2(t) = [B_{02}(t), B_{12}(t), B_{22}(t)]^T$ is a vector of Bernstein polynomials of degree 2. By combining this with Equation 2.42 it is possible to write the following (where $\dot{\mathbf{G}}_{B3}^{g,e}(k) = [\dot{G}_{B1}^{g,e}(k), \dot{G}_{B2}^{g,e}(k), \dot{G}_{B3}^{g,e}(k)]^T$ is a vector of Bernstein ramping coefficients):

$$\dot{\mathbf{G}}_{B3}^{g,e}(k) = \mathbf{M}\mathbf{G}_H^{g,e}(k) \tag{2.46}$$

where $\mathbf{M}$ is the matrix

$$\mathbf{M} = \mathbf{K}^T\mathbf{W}^T = \begin{bmatrix} 0 & 1 & 0 & 0 \\ -3 & -1 & 3 & -1 \\ 0 & 0 & 0 & 1 \end{bmatrix} \tag{2.47}$$

Equation 2.46 relates the ramping coefficients of the Bernstein formulation with the Hermite spline coefficients through the Matrix in 2.47. Now that both the Bernstein load and Bernstein ramping trajectory coefficients are expressed in terms of Hermite spline coefficients, the *Bernstein convex hull* property can be used to defined generating and ramping constraints.

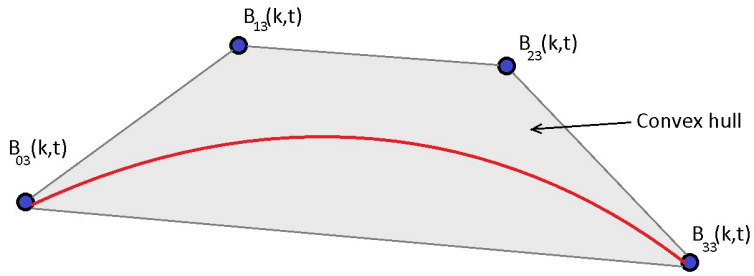

Figure 2.4: The Bernstein Convex Hull

2.6.4 Bernstein Convex hull

A very important characteristic of Bernstein polynomials is their convex hull property, which yields that the value of the polynomial at any time t is bounded by the minimum and maximum Bernstein coefficients[30]. This means that maximum and minimum power and ramping capacities for thermal and ES units can be constrained by the Bernstein convex hull property.

Figure 2.4 shows an example of a Bernstein convex hull given 4 data points. The interpolated curve is always contained by this hull, hence the complex hull can be used to define operating conditions for the thermal and ES units. Power output constraints are:

$$\max(G^g_{B03}(k), G^g_{B13}(k), G^g_{B23}(k), G^g_{B33}(k)) \leq P^{max}_g(U(t,g) + Z(t,g)) \quad (2.48)$$

$$\min(G^g_{B03}(k), G^g_{B13}(k), G^g_{B23}(k), G^g_{B33}(k)) \geq P^{min}_g(U(t,g) - Y(t,g)) \quad (2.49)$$

$$\max(G^e_{B03}(k), G^e_{B13}(k), G^e_{B23}(k), G^e_{B33}(k)) \leq P^{max}_e \quad (2.50)$$

$$\min(G^e_{B03}(k), G^e_{B13}(k), G^e_{B23}(k), G^e_{B33}(k)) \geq P^{min}_e \quad (2.51)$$

, while the ramping constraints are

$$\max(\dot{G}^g_{B1}(k), \dot{G}^g_{B2}(k), \dot{G}^g_{B3}(k)) \leq SU_g Y(t,g) + RU(U(t,g) - Y(t,g) + Z(t,g)) \tag{2.52}$$

$$\min(\dot{G}^g_{B1}(k), \dot{G}^g_{B2}(k), \dot{G}^g_{B3}(k)) \geq RD_g U(t,g) + SD_g Z(t,g) \tag{2.53}$$

$$\max(\dot{G}^g_{B1}(k), \dot{G}^g_{B2}(k), \dot{G}^g_{B3}(k)) \leq RU_e \tag{2.54}$$

$$\min(\dot{G}^g_{B1}(k), \dot{G}^g_{B2}(k), \dot{G}^g_{B3}(k)) \geq RD_e \tag{2.55}$$

Equation 2.48 defines upper and lower boundaries of the convex for generating output, while Equation 2.52 defines upper and lower ramping limits. Notice how the convex hull of the generating trajectories has 4 data points, while the convex hull of the ramping trajectories has 3 data points. This is because the convex hull of a n degree Bernstein polynomial is defined by $n+1$ data points.

2.6.5 UC model vairables

The Bernstein UC model has 3 logical variables per thermal unit, and 4 variable denoting the power trajectory of hourly power flow. The ES units have 9 variables per hourly interval, 4 denoting charging power trajectory, 4 denoting discharging power trajectory and one for ES state of charge.

Chapter 3

Test System

Method

The proposed Bernstein UC formulation in this model will be assessed using the 1996 IEEE 24-bus RTS, with data from [1] and [31]. The schematic of the test system is shown in Figure 3.1. All load data that will be used in the test will be scaled to a maximum value of 2850 MW, which is the maximum generating capacity of the system. Load data used for simulations in this thesis is from CAISO[32]. Simulations are done in two stages, where the DA UC scheduling costs are calculated as a first step before the RT economic dispatch is simulated in stage two.

For each load data simulation, the Bernstein UC models will be solved using the submodels:

- Standard UC formulation
- Robust UC formulation
- Standard UC formulation with ES units
- Robust UC formulation with ES units

Data for the ES units is presented in this chapter, while the robust UC model constraints are presented in Chapter 4.

To asses the performance of the proposed UC model, the operation costs of the proposed Bernstein-polynomial based model will be compared to the same

simulation on a traditional UC model. This comparison will be used not only for a purely cost-based side-by-side comparison but will also be used to evaluate potential ramping scarcity in the UC models.

3.1 Important simplifications and definitions

Auxiliary power generating units that may be employed during the real-time operation of the system respond on demand, and will thus not have associated commitment restrictions. IEEE 24-Bus RTS load bus and transmission line ratings are listed in Appendix B.

The day-ahead UC models in this thesis will operate under the following assumptions and simplifications:

1. All generating units in the system will operate with the DA determined commitment status. Power output, however, can be regulated to meet the load demand in the system.

2. ES units will operate under the day-ahead operating schedule. The charging/discharging cycles of the ES units will be determined from the DA scheduling, independent of RT load demands. Hence, all response to real-time load deviations will be done by generating and auxiliary units only.

3. If the load demand or ramping of the load exceeds the capacity of the committed generating units and ES units in the system at any point, the extra power is supplied by auxiliary generating units that respond to demand in RT. It is assumed that there is always enough power available from these auxiliary units to meet the net load demand in the system.

4. To avoid modifications of load distribution and transmission line data, it is assumed that all power from VRES reduces net load uniformly for the entire load bus system.

5. The system is assumed to have a power factor equal to 1. This means that the thermal limits of transmission lines between buses (see Figure 3.1) given in MVA can be considered in MW.

6. Resistive losses in transmission lines are ignored, and it is assumed that power can flow freely in any direction in the transmission lines, within the thermal limits of the transmission.

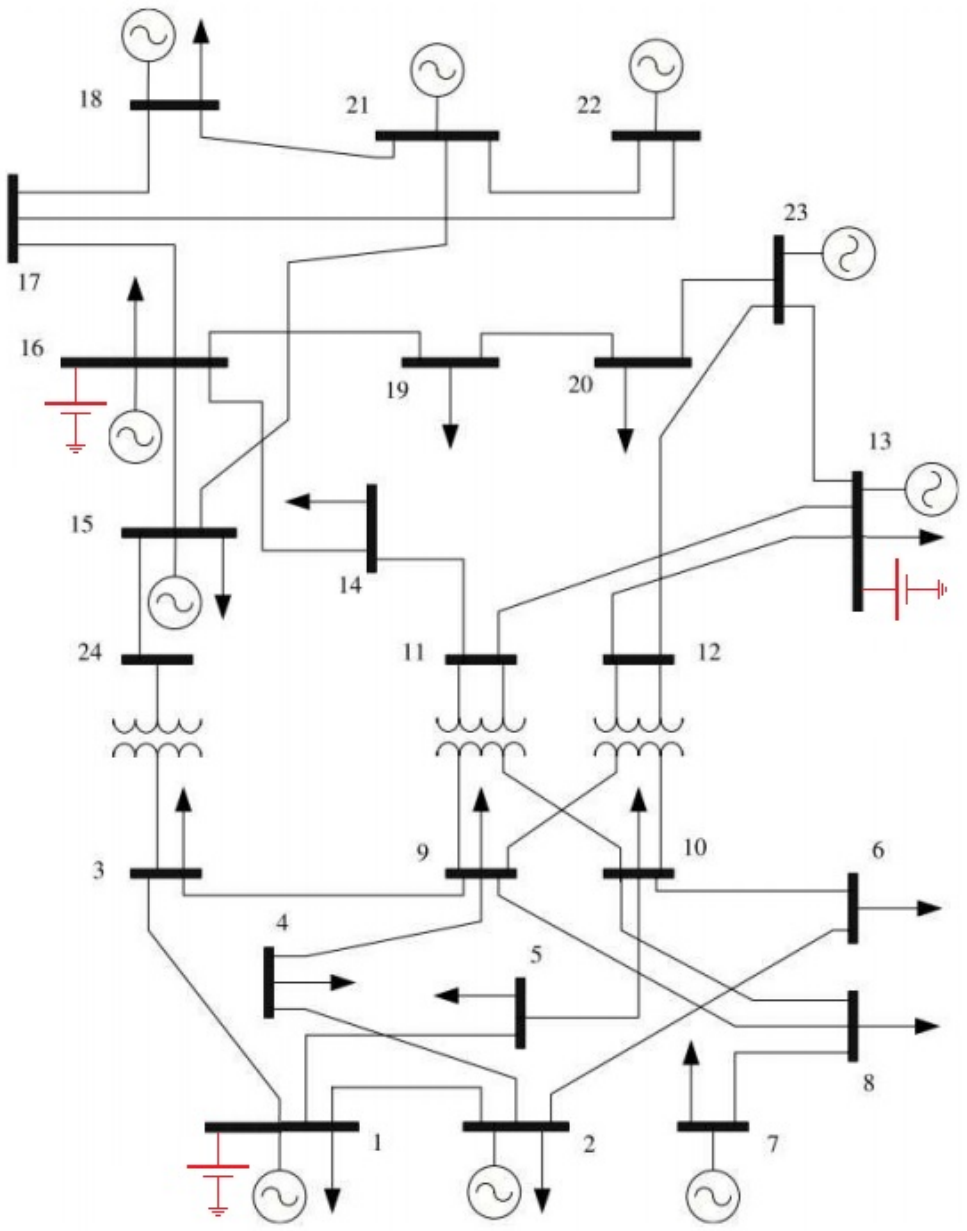

Figure 3.1: The IEEE 1996 Reliability Test System[1] with added ESS units at buses 1, 13 and 16

A change in load demand will affect the net output of the generating units in the systems. But as transmission lines have given thermal limits, it may be necessary to re-direct the flow directions and hence also power generation in the system. This is mainly a consideration when the RT demand is significantly higher than the day-ahead forecasted demand. These potential extra costs are accounted for and considered in the real-time UC model.

The test system that will be used for this paper is the IEEE 24-Bus RTS, with 32 generating units distributed over a total of 12 buses. The generating units will be considered on a per-bus basis, i.e. 12 generating buses, denoted by $g_1, ..., g_{12}$, and their characteristics are listed in the table below. Additionally, a bulk auxiliary generating unit has been added. This unit will not be considered for the day-ahead scheduling of UC, but will only serve during the RT calculations of system operation costs, to supply the ramping and generating capacity the committed generating units cannot supply themselves.

3.2 Generating Units

The auxiliary generating unit will be considered as one bulk unit and denotes all auxiliary power that has been supplied to the system during operation. The generating unit data used in this paper is based on on [1],[31], [33] and [34], and is listed in Table 3.1.

The marginal cost for auxiliary generating units has been capped at 40 MW/h which is greater than the marginal costs of all 12 generating units in the 24-Bus system. This has been determined such that the expensive auxiliary generating unit will only be called on to keep the generation-demand balance in the system from becoming infeasible. A poorly constructed UC formulation model may need great amounts of auxiliary generation, and will hence have high operation-costs, which is not desirable.

As generating units have minimum up- and down times, their operation status at the beginning of the scheduling period is important. The commitment status and current ontime/downtime in Table 3.1 has been randomly selected such that available generating capacity in the system at the beginning of the scheduling interval is sufficient to meet standard (and robust) generating constraints.

Gen. Unit	a ($/MW^2$)	b ($/MW$)	c ($)	C_{SD} ($)	C_{SU} ($)	RU (MW/h)	RD (MW/h)	UT (h)	DT (h)
g1	0	13.32	0	1430.4	1430.4	120	120	8	4
g2	0	13.32	0	1430.4	1430.4	120	120	8	4
g3	0	20.70	0	1725	1725	350	350	8	8
g4	0	20.93	0	3056.7	3056.7	240	240	12	10
g5	0	26.11	0	437	437	60	60	4	2
g6	0	10.52	0	312	312	155	155	8	8
g7	0	10.52	0	312	312	155	155	8	8
g8	0	6.02	0	0	0	280	280	1	1
g9	0	5.47	0	0	0	280	280	1	1
g10	0	0	0	0	0	300	300	1	1
g11	0	10.52	0	624	624	180	180	8	4
g12	0	10.89	0	2298	2298	240	240	8	4
g_{aux}	0	40	0	x	x	x	x	x	x

Gen. Unit	SD (MW/h)	SU (MW/h)	P_{min} (MW)	P_{max} (MW)	U_0 (h)	U_{ini} (0/1)	S_0 (h)	CU ($/MW)	CD ($/MW)	Bus
g1	120	120	30.4	152	22	1	0	15	14	1
g2	120	120	30.4	152	22	1	0	15	14	2
g3	350	350	140	350	0	0	20	10	9	7
g4	240	240	206.65	591	22	1	0	8	7	13
g5	60	60	12	60	0	0	10	7	5	15
g6	155	155	54.25	155	0	0	20	16	14	15
g7	155	155	54.25	155	10	1	0	16	14	16
g8	280	280	100	400	50	1	0	0	0	18
g9	280	280	100	400	16	1	0	0	0	21
g10	300	300	0	300	24	1	0	0	0	22
g11	180	180	108.5	310	10	1	0	17	16	23
g12	240	240	75	350	50	1	0	16	14	23
g_{aux}	x	x	x	x	0	0	0	x	x	x

Table 3.1: Generator data used for UC optimization

a	Quadratic generating cost	SU	Maximum startup ramping
b	Linear generating cost	P_{min}	Minimum output power
c	Fixed generating cost	P_{max}	Maximum output power
C_{SD}	Shutdown costs	U_0	Current ontime
C_{SU}	Startup costs	U_{ini}	Initial commitment status
RU	Maximum ramp up rate	S_0	Current offtime
RD	Maximum ramp down rate	CU	Upward reserve cost
UT	Minimum uptime	CD	Downward reserve cost
DT	Minimum downtime	Bus	Location of generating unit
SD	Maximum shutdown ramping		

Table 3.1 shows the generating unit data the will be used for the UC problem. Note that all fixed commitment costs and quadratic generating costs are set to be zero. Generating units g_8, g_9 and g_{10} do not have any startup- or shutdown costs, and additionally generating unit g_{10} is the only unit without any lower boundary for power output. The buses are located as shown in Figure 3.1, and their operation is constrained by the thermal limits of the lines between the buses.

3.3 Energy Storage Systems

Although ES units are not a part of the original IEEE 24-Bus RTS, three ESS units have been added to some of the UC case studies in this thesis, to better represent a modern power grid. The 3 ES units have been placed on bus 1, 13 and 16. The ES units placed on bus 1 and 16 are two identical lithium-ion battery banks, with energy storage capacities of 100MWh and rated power of 100 MW. The ES unit on bus 13 is a pumped hydro storage system, with a rated capacity and power of 1000 MWh and 250 MW, respectively.

The ES unit data is retrieved from [24], and ramping rate specifications are based on data from [35] and [20]. Batteries are prone to degradation, and their health is highly sensitive to charging and discharging patters. It is not good practice to have discharging cycles between a full state of charge and no state of charge, as this will accelerate degradation significantly and reduce the battery lifetime[36]. However, for this UC model formulation, assume that the SOC describes the available capacity in the battery, where degradation has been taken into account.

ESS Unit	RU (MW/h)	RD (MW/h)	P_{max} (MW)	P_{min} (MW)	E_{max} (MWh)	E_{ini} (MWh)	η_c	η_d	Bus
es1	2000	2000	100	-100	100	0	0.95	0.95	1
es2	1500	1500	250	-250	1000	0	0.90	0.90	13
es3	2000	2000	100	-100	100	0	0.95	0.95	16

Table 3.2: ESS data used for UC optimization

RU	Maximum ramp up rate	E_{ini}	Initial energy
RD	Maximum ramp down rate	η_c	Charging efficiency
P_{max}	Maximum output power	η_c	Discharging efficiency
P_{min}	Minimum output power	Bus	Location of ESS unit
E_{max}	Maximum storage capacity		

Table 3.2 shows the ES unit specs for the UC model used in this paper. The parameter E_{ini} describes the initial energy in a given ES unit. A constraint that has been used in [37] is that the SOC of all ESS units at the end of the scheduling interval is equal to the initial SOC at the beginning of the scheduling interval. The same constraint will be used in this UC model:

$$E_{end} = E_{ini} \tag{3.1}$$

The term E_{end} in Equation 3.1 is the energy in a ESS unit at the end of the scheduling period. This constraint ensures that all ESS units are ready to operate under the same conditions in every scheduling interval. The charging/discharging cycles of the ESS units are unrestricted.

3.4 RT operation costs

CAISO load data is given in hourly intervals for the day-ahead load forecasts, and averaged values in 5-minute intervals for the RT load demand data. Hence, the RT economical dispatch will be simulated in 5-minute intervals. The RT operation cost function is given in 2.20, accounting for the cost of shredded load and curtailed VRES. For the UC simulations in this thesis, no load needs to be shredded and no VRES needs to be curtailed. Thus, the RT operation cost function for 5-minute dispatch window becomes:

$$C_{RT} = \sum_{g,t}(CU_g \Delta G_g^+(t) + CD_g \Delta G_g^-(t)) + \sum_{aux,t} c_{aux} G_{aux}(t) \tag{3.2}$$

As shown in Equation 3.2, the RT operation costs is now a function of up/down reserve deployment per generating unit and auxiliary generation. The RT operation constraints are an extension of the UC operations constraints listed in Chapter 2, restricting both generating output and ramping. The generating output power constraints are:

3.4.1 Bernstein UC RT operation

$$G_g^{DA}(t) + \Delta G_g^{+}(t) + \Delta G_g^{-}(t) \leq P_g^{max}(U(t,g) + Z(t,g)) \tag{3.3}$$

$$G_g^{DA}(t) + \Delta G_g^{+}(t) + \Delta G_g^{-}(t) \geq P_g^{min}(U(t,g) - Y(t,g)) \tag{3.4}$$

$$\begin{aligned}&(G_g^{DA}(t) + \Delta G_g^{+}(t) + \Delta G_g^{-}(t)) - (G_g^{DA}(t-1) + \Delta G_g^{+}(t-1) + \Delta G_g^{-}(t-1)) \\ &\leq \frac{RU_g}{12}(U(t,g) - Y(t,g) + Z(t,g)) + \frac{SU_g}{12}Y(t,g)\end{aligned} \tag{3.5}$$

$$\begin{aligned}&(G_g^{DA}(t) + \Delta G_g^{+}(t) + \Delta G_g^{-}(t)) - (G_g^{DA}(t-1) + \Delta G_g^{+}(t-1) + \Delta G_g^{-}(t-1)) \\ &\geq \frac{RD_g}{12}U(t,g) + \frac{SD_g}{12}Z(t,g)\end{aligned} \tag{3.6}$$

Equation 3.3 and Equation 3.4 constrain the generating reserves that are available per thermal unit as a function of the day-ahead scheduled operation. Equation 3.5 and Equation 3.6 define the ramping constraints of the thermal units as averaged values in 5-minute intervals, in correspondence with the RT load dispatch data from CAISO.

3.4.2 Traditional UC RT operation

$$G_g^{DA}(t) + \Delta G_g^{+}(t) + \Delta G_g^{-}(t) \leq P_g^{max}U(t,g) \tag{3.7}$$

$$G_g^{DA}(t) + \Delta G_g^{+}(t) + \Delta G_g^{-}(t) \geq P_g^{min}U(t,g) \tag{3.8}$$

$$(G_g^{DA}(t) + \Delta G_g^+(t) + \Delta G_g^-(t)) - (G_g^{DA}(t-1) + \Delta G_g^+(t-1) + \Delta G_g^-(t-1))$$
$$\leq \frac{RU_g}{12}(U(t,g) - Y(t,g)) + \frac{SU_g}{12}Y(t,g), \text{ if } U(t-1,g) = 1 \text{ and } U(t,g) = 1 \tag{3.9}$$

$$(G_g^{DA}(t) + \Delta G_g^+(t) + \Delta G_g^-(t)) - (G_g^{DA}(t-1) + \Delta G_g^+(t-1) + \Delta G_g^-(t-1))$$
$$\geq \frac{RD_g}{12}U(t,g), \text{ if } U(t-1,g) = 1 \text{ and } U(t,g) = 1 \tag{3.10}$$

$$(G_g^{DA}(t) + \Delta G_g^+(t) + \Delta G_g^-(t)) - (G_g^{DA}(t-1) + \Delta G_g^+(t-1) + \Delta G_g^-(t-1))$$
$$\leq SU_g, \text{ if } U(t-1,g) = 0 \text{ and } U(t,g) = 1 \tag{3.11}$$

$$(G_g^{DA}(t) + \Delta G_g^+(t) + \Delta G_g^-(t)) - (G_g^{DA}(t-1) + \Delta G_g^+(t-1) + \Delta G_g^-(t-1))$$
$$\leq SD_g, \text{ if } U(t-1,g) = 1 \text{ and } U(t,g) = 0 \tag{3.12}$$

Equation 3.3 and Equation 3.4 restrict the output from thermal units during commitment hours. Equation 3.9 and Equation 3.10 restrict ramping during commitment hours. Equation 3.11 and Equation 3.12 restrict the ramping during startup and shutdown sequences. Notice that the startup and shutdown ramping constraints for the Bernstein UC formulation are tighter than for the traditional UC model, as the two models have a different startup and shutdown syntax.

Chapter 4

Robust Optimiaztion

4.1 Background

Robust UC models have gained much attention in recent years[38]. Robust optimization uses uncertainty sets, assuming the true probability distributions of the uncertainty parameter to be unknown. A basic robust optimization problem uses hard constraints, such that no realization of the unknown data set can violate the constraints. The authors in [39] propose a contingency constrained UC model, that schedules UC to be able to handle simultaneous worst-case contingencies at once, and thereby inflicting very conservative robust UC uncertainty sets.

A more sophisticated approach to robust optimization is to restrict the uncertainty sets. This can help eliminate the most extreme realizations of an uncertainty set[40]. Certain realizations are assumed very unlikely to occur and can impose very tight bounds. Hence it is reasonable to restrict such extreme realizations by using softer uncertainty sets.

In [41] a robust UC model is constructed with a 95% confidence interval for the uncertainty sets, and in [42] a 90% confidence interval is used. In papers [43][44][41] and [42] the authors discuss the advantages of using elements of stochastic optimization in robust optimization, and in all of these papers, historical load data is used to design appropriate uncertainty sets. This approach will also be used for the robust UC model in this thesis.

Figure 4.1 shows two uncertainty set as function of x- and y-variables. Let the square be the "primary" set and the ellipse another uncertainty set that

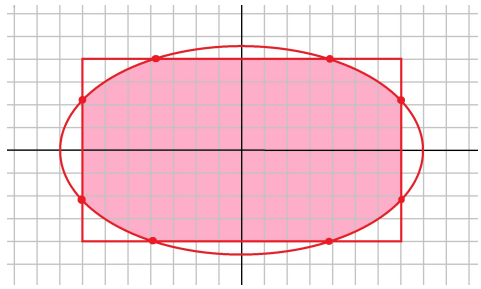

Figure 4.1: Example of Uncertainty Sets for Robust Optimization

has been introduced to restrict possible realizations of the net uncertainty set. Any possible realization of the uncertainty set is the pink area inside both the rectangle and the ellipse. The most extreme realizations of the uncertainty set that would have been the corners of the red square are now eliminated, and the extreme cases are now at the intersection points of the curve and the rectangle. This is just an example of how a combination of the variables in x-direction and y-direction can be restricted by selecting appropriate uncertainty sets.

4.2 The Unit Commitment problem

A crucial part of scheduling generators to meet demands in a UC problem is to achieve economic savings[45]. Another critical aspect is maximizing the efficiency of the real-time operation of power systems, as the cost of electricity is linked directly with the efficiency of power systems[46]. In recent years, power systems have experienced a significant increase in the penetration level of VRES. This has contributed to lower power production costs, but perhaps more importantly, it helps reduce carbon emissions.

However, VRES provide major challenges in the scheduling of power systems operations, as the power output of renewables cannot be predicted accurately in the day-ahead planning [47][48]. Another problem with VRES such as wind and solar is the magnitudes of the variations, which yields the need for fast-ramping capacity in power systems[49][50]. To maintain system stability in power systems with increasing uncertainties, it may hence be necessary to design Robust UC problem formulations.

The day-ahead UC problem formulation deals with two main uncertainty parameters, namely, load forecast uncertainty and VRES output uncertainty. In

systems dominated by thermal and hydro generating units and low penetration of VRES, the uncertainty parameter of biggest concern is the load forecast. The trend in current and future power systems is increasing penetration of VRES, and it has become increasingly important to establish VRES output forecast models. In this thesis, two separate forecast uncertainty sets will be determined, one for the load forecast, and one for the VRES output forecast. Finally, the two uncertainty sets will be merged into one single uncertainty set.

4.3 Robust Load Forecast Model

The worst case scenarios that will be used to make appropriate uncertainty sets for the robust load forecast model are based on historical load data from CAISO. Load data from the full month of February 2019 will be analyzed to determine the following:

- Maximum day-total deviation from forecasted generating schedule, relative to the total load demand in the system
- Peak deviations relative to peak demand in the system
- Hours of a day with large deviations from forecasted generating schedule. This robust model will consider any deviation larger than 2/3 of the peak deviation, as a large deviation.
- Investigate any possible correlations between forecast error and: peak load, time of the day or load ramping. If any relation, this will be used to define the base for the robust constraints.

4.3.1 Analysis of February 2019 CAISO Load Data

The data analysis is divided into to main parts: The first part of the analysis will investigate if the day-ahead forecasting error can be linked to the following: 1) Amplitude of the load, 2) Time of the day, and 3) Ramping of the load. The second part of this analysis will be used to determine numerical values for the uncertainty sets.

Observations

In Figure 4.2, the orange curve shows the accumulated loads for the entire month of February 2019, scaled down to a maximum value of 100 MW. The blue curve

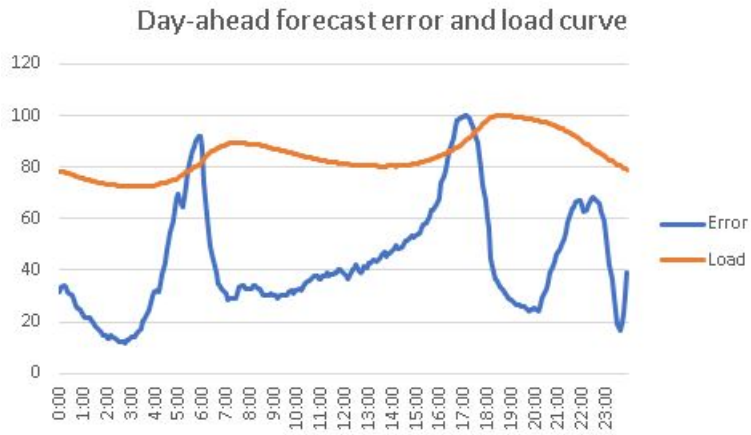

Figure 4.2: Day-ahead forecast error and load curve scaled down to maximum values of 100 MW

shows the accumulated forecast errors for the same time period, scaled down to a maximum value of 100MW. There seems to be little correlation between peak load and forecast errors, and similarly, there seem to be no clear trends in the errors related to time of the day (e.g. no linear change in errors related to the time of the day). However, there seems to be a relation between the load ramping and the forecast errors. The figure shows peaks in forecast errors where the load has the steepest ramps.

Another observation that can be made is that there are two main peak loads in Figure 4.2 one occurring at the morning hours at about 7:00 AM and another one at about 6:00 PM. This is a very typical profile, as discussed in [51] and [52], with one peak occuring at between hour 0:00 PM-11.59 AM and another one between 12.00 AM-11.59 PM. Steep ramping of the load curve is often related to the ramp up and down from these peaks.

To investigate the load ramping hypothesis further, Figure 4.3 shows the forecast error on the y-axis plotted versus the load ramping on the x-axis. The absolute value of the forecast errors is plotted, i.e. the graph does not distinguish between negative or positive forecast errors but only shows the magnitude of the errors.

The forecast errors in Figure 4.3 are scattered over a large area, indicating a large standard deviation for forecast errors. However, it is possible to observe

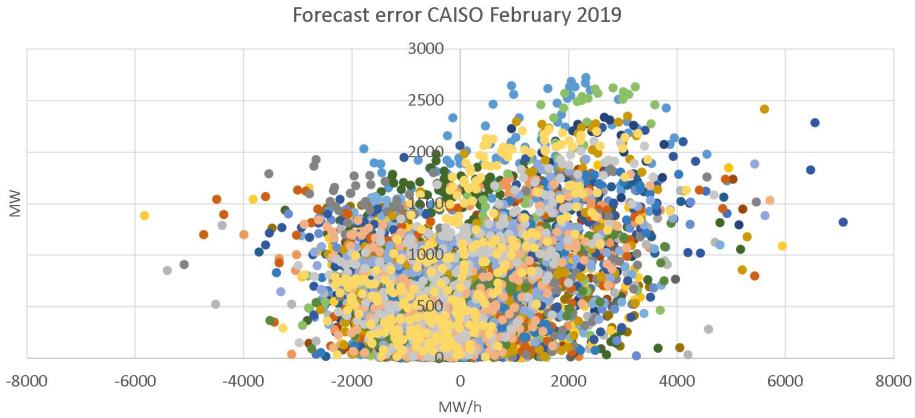

Figure 4.3: Forecast error plotted versus ramping of load

a trend in increasing forecast errors with steeper load ramping, which supports the observation made from Figure 4.2, where there appears to be a correlation between forecast errors and ramping.

Numerical Data

Step two of the Robust UC problem formulation is to identify the numerical values for the uncertainty sets. The first parameter to be determined is the total forecast error for a day divided by the total load demand for the same day. The next parameter to be determined is the fraction of errors for a given day that is upward and downward errors, i.e. when the forecasted load curve is greater/lower than the real-time demand curve. The maximum robust boundaries for a given load curve will be calculated by determining the worst case forecast error of the load profile, and dividing it by the peak load demand the same day. The last parameter to be determined is the period during a day at which a large forecast error has occurred. As discussed above, a large forecast error in this model will be defined as any deviation larger than 2/3 of the peak deviation.

Date	Error	Fraction of error pos.	Fraction of error neg.	Peak error/ peak load	Fraction with large error
February 1.	1.7%	24.1%	75.9%	6.1%	6.3%
February 2.	2.0%	33.2%	66.8%	4.4%	22.2%
February 3.	2.4%	52.2%	47.8%	5.9%	5.6%
February 4.	2.4%	25.0%	75.0%	6.8%	10.4%
February 5.	**4.4%**	6.2%	**93.8%**	9.9%	24.0%
February 6.*	3.7%	10.6%	89.4%	**14.9%**	5.9%
February 7.	2.6%	23.9%	76.1%	8.5%	10.1%
February 8.	2.4%	7.5%	92.5%	6.7%	10.4%
February 9.	2.1%	60.6%	39.4%	4.4%	16.3%
February 10.	2.4%	75.3%	24.7%	5.4%	14.2%
February 11.	2.5%	34.5%	65.5%	6.6%	13.9%
February 12.	3.5%	**85.8%**	14.2%	7.2%	**33.0%**
February 13.	2.2%	67.3%	32.7%	5.9%	15.6%
February 14.	2.8%	38.1%	61.8%	6.4%	18.8%
February 15.	2.8%	37.7%	62.3%	6.0%	14.2%
February 16.	2.4%	81.9%	18.1%	6.0%	11.5%
February 17.	2.1%	49.6%	50.4%	5.7%	11.8%
February 18.	2.9%	18.5%	81.5%	9.6%	9.4%
February 19.	2.8%	49.4%	50.6%	8.3%	7.3%
February 20.	2.4%	49.8%	50.2%	6.5%	18.8%
February 21.	2.7%	66.6%	33.4%	7.0%	16.3%
February 22.	3.0%	34.5%	65.5%	8.8%	9.7%
February 23.	2.4%	46.1%	53.9%	6.6%	10.8%
February 24.	2.2%	16.4%	83.6%	4.8%	20.8%
February 25.	3.3%	15.9%	84.1%	7.0%	17.0%
February 26.	2.3%	38.0%	62.0%	6.5%	14.6%
February 27.	3.6%	12.4%	87.6%	7.7%	14.6%
February 28.	4.0%	10.0%	90.0%	8.1%	25.0%
Maximum	**4.4%**	**85.8%**	**93.8%**	**14.9%**	**33.0%**

Table 4.1: Error data for February 2019 CAISO Load Data

Uncertainty Sets

By calculating the parameters in Table 4.1 as fractions, they can easily be applied to any load curve, which is what will be done for the robust formulation used for the UC problem in this thesis. As discussed in the introduction of this chapter, the next step for the Robust optimization problem is to use the data from Table 4.1 to determine appropriate uncertainty sets for the robust UC formulation.

The worst possible day-total error occurs on February 5. with a total forecast error of 4.4%. The robust constraint in thus paper will be set at 15% to ensure that all errors in Table 4.1 is contained in the uncertainty set. Another takeaway is the fractions of the total errors that are positive/negative errors, respectively. On February 12., 85.5% of the error was positive errors (RT load greater than forecasted load), while on February 5., 93.9% of the errors were negative errors (real-time load lower than forecasted load). For the rest of the month the ratio between positive and negative errors varies, some days negative errors dominate, other days positive errors dominate. For the uncertainty set, it is hence assumed that 100% of the error can occur in either direction.

The peak error in the forecasts occurs on February 6, with a peak error of 14.9%. An important note here, however, is that the CAISO load data for this particular day may be faulty. Between 5.00PM and 6.00Pm there is a sudden load drop before the normal load curve shape resumes after 6.00PM. The peak error for all other days is well below 10%. Hence, 9% of the total peak will be used as the benchmark upper error for the uncertainty set.

The last parameter that will be used is the fraction of the day where large errors occur. As mentioned above, these are all errors greater than 2/3 in magnitude of the peak error for the day. On February 12., this occurs for 33% of the scheduling period, which translates to 8 hours. The uncertainty set in this Robust Optimization problem will thus be that the peak error of 15% of the curve max can occur for 8 hours, in both a negative an positive direction. As the upper bound for day-total error is determined to be at 5%, the remaining 16 hours of the 24-hour scheduling time frame, where peak-error doesn't occur, will have error bounds such that the day-total allowed error sums up to 5%.

Table 4.2 sums up all parameters that make up the uncertainty set for the Robust UC optimization problem, based on February 2019 CAISO load data. Notice how the peak-error is assumed for only 8 hours per day, to narrow down the uncertainty set. As discussed in the introduction of this chapter, these are not hard constraints but are valid when there's a very low probability of extreme realization of uncertainties, as e.g. large errors occurring for an entire 24 hours

Robust Optimization Uncertainty Set				
Total Error	Fraction of error pos.	Fraction of error neg.	Peak error/ peak load	Hours with large error
15%	100%	100%	9%	8

Table 4.2: Robust Uncertainty set for UC model

of a day.

The uncertainty bounds are calculated as follows:

$$\Delta N_k^{R,max} = 9\% \cdot \max N(t) \tag{4.1}$$

$$\int_0^{24} \Delta N_k^R(t)dt = 15\% \cdot \int_0^{24} N(t)dt \tag{4.2}$$

In Equation 4.1, $\Delta N_k^{R,max}$ is the upper uncertainty bound. The lower uncertainty bound is calculated such that Equation 4.2 is fulfilled. For all intervals that are not peak-errors intervals, $\Delta N_k^R(t)$ is uniformly distributed. This will be illustrated with examples below. A model that determines the 8 peak-error intervals will also be addressed below. And, finally, as it assumed that 100% of the forecast error can occur in both a negative and positive direction, the following can be stated:

$$\Delta N_k^{R,up}(t) = 100\%\Delta N_k^R(t) = \Delta N_k^R(t) \tag{4.3}$$

$$\Delta N_k^{R,down}(t) = 100\%\Delta N_k^R(t) = \Delta N_k^R(t) \tag{4.4}$$

Equations 4.3 and 4.4 can be modified such that the error bounds for a given system become asymmetrical and shifted in either a positive or negative direction. However, as seen from Table 4.1, the errors shift from positive to negative day by day, hence this thesis will consider symmetric error bounds.

Integrating ramping into the Robust Optimization model

As discussed above, based on the observations and interpretations of Figure 4.2 and Figure 4.3, there seems to be a correlation between load ramping and forecast errors. The ramping periods of the load, are related to the peak load demands throughout the day. Again, as discussed above, there are typically

two peak demands points throughout the day, one occurring between 0:00PM-11.59AM and another one between 12.00AM-11.59PM.

As the uncertainty set is determined to account for 8 hours of peak error, it is reasonable to assume that 4 of these errors will occur around each peak-load. Hence this uncertainty set will designate 4 max-error hours between 0:00PM-11.59AM and 4 between 12.00AM-11.59PM. The 4 hours for each time intervals will be divided into two, where 2 maximum-peak errors will form uncertainty bounds for the two hours with the larges ramping-up and the remaining two for the two hours with the greatest ramping down. This uncertainty set will be used to determine both the negative and positive uncertainty bound for the load forecast trajectory.

4.3.2 Determining uncertainty boundaries

Now that the robust load uncertainty set has been defined, it can be applied to the load demand data that will be used of the UC problem formulation in this thesis. As two main UC formulations are discussed in this paper, namely the continuous time Bernstein-model and the traditional hour-to-hour constant model. This means that the Robust uncertainty sets have to be applied slightly differently for the models.

The uncertainty bounds will be used to define robust generating constraints by considering the generating capacity of the committed generating unit in the system:

$$U(t,g)P_g^{max} + \sum_e G_e(t) \geq N^k(t) + \sum_e D_e(t) + \Delta N_k^R(t) \tag{4.5}$$

$$U(t,g)P_g^{min} + \sum_e G_e(t) \leq N^k(t) + \sum_e D_e(t) - \Delta N_k^R(t) \tag{4.6}$$

Equation 4.5 simply states that the generating capacity of the committed generating units at any given time in the system must be greater than the forecasted load plus uncertainty boundaries. Similarly, Equation 4.6 states that the minimum output of all committed units must be lower than forecasted load minus uncertainty boundaries.

The peak values of the uncertainty sets are the same for both models. However, the uncertainty bounds for the Bernstein model will be described by Bernstein coefficients and will enforce continuity. For the Bernstein model, the interval between a peak-error interval and a non-peak interval will be an interval where the uncertainty bounds ramp between peak and non-peak. This will

be illustrated in the figures below. The traditional UC model has no continuity constraints and will have separate bounds for peak-error intervals and non-peak-error intervals.

To illustrate how the uncertainty bounds will be applied to a load curve, CAISO load data from an arbitrary day can be selected. A day with relative large forecast errors and ripple is May 4th, 2018, which will be used here as an example. First, the data will be scaled down to the IEEE RTS maximum of 2850 MW. The results are shown in the figures and discussed below.

The Bernstein Load model

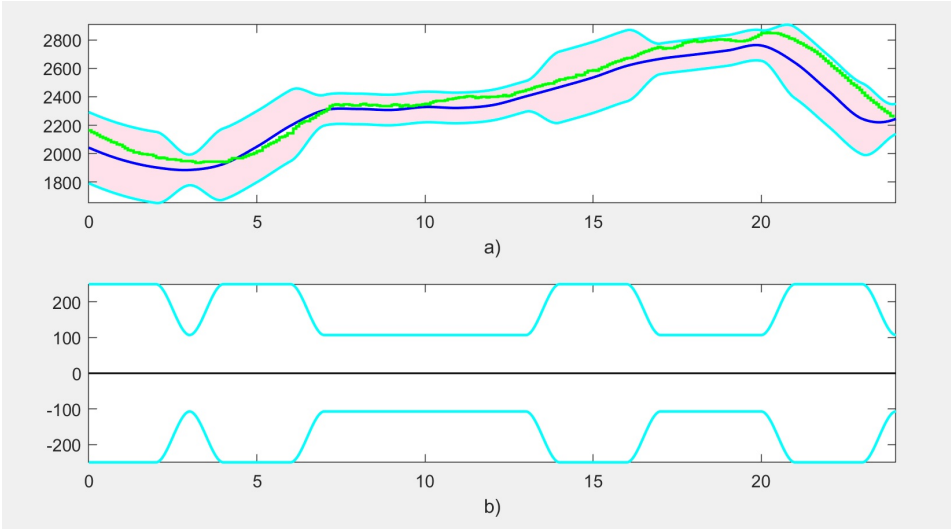

Figure 4.4: Uncertainty boundaries for Robust UC

In Figure 4.4, first consider plot *a)*. The dark blue curve shows the day-ahead forecasted load, while the green curve is the real-time load. The cyan curves are the uncertainty boundaries calculated from the day-ahead forecasted load. As shown in plot *b)*, the uncertainty curves are identical with respect to negative and positive errors, and are added as constraints on top of the forecasted load curve as shown in plot *a)*. Notice that the RT load curve is captured by the robust boundaries. The ramping at the hour-interval points is defined to be zero.

The traditional UC model

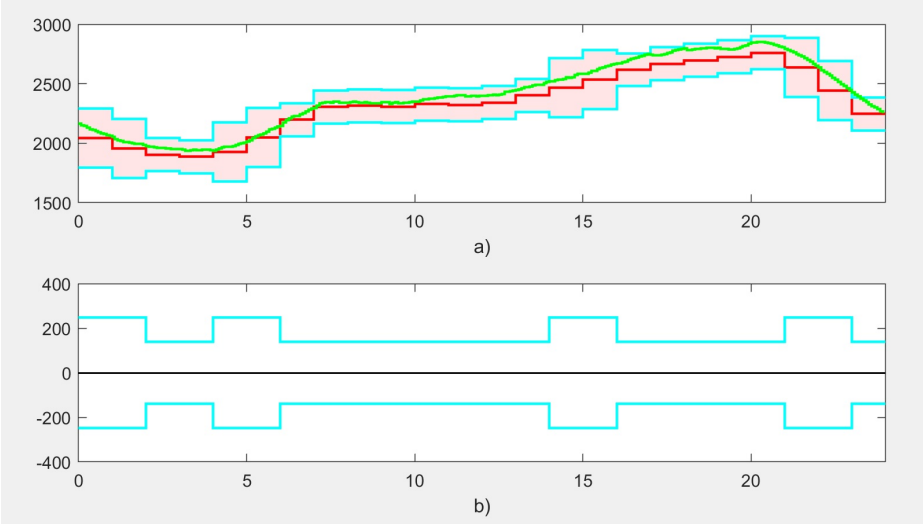

Figure 4.5: Uncertainty boundaries for Robust UC

In Figure 4.5, first consider plot *a)*. The red curve shows the day-ahead forecasted load, while the green curve is the real-time load. The cyan curves are the uncertainty boundaries calculated from the day-ahead forecasted load. As shown in plot *b)*, the uncertainty curves are identical with respect to negative and positive errors, and are added as constraints on top of the forecasted load curve as shown in plot *a)*. Notice that the real-time load curve is captured by the robust boundaries for almost the entire time frame, except from a small deviation in the interval 11:00 PM - midnight.

4.4 Robust VRES Forecast Model

Designing an efficient VRES forecast model is a challenging problem, but likewise an essential element in integrating VRES into power system operations. A number of advanced forecast models are evaluated in [53], and reflect that wind power forecasting is highly dependent on typography, climate and a number of other parameters. The most accurate forecast models are also the most complex

ones and may require a large number of input parameters. Due to the limited availability of historical CAISO VRES forecast data, some simplifications are needed for the VRES forecast model in this thesis.

In [54], a stochastic UC model is designed and evaluated, using a two-stage UC approach. In stage one, the traditional day-ahead UC scheduling is carried out to determine the next-day commitment scheduling of slow-start generating units. Step two is carried out inside the scheduling horizon, using *rolling planning*. RT VRES generating data is used to generate scenario trees[55], and the UC problem is resolved and updated intra-period, using data from the scenario trees as inputs. The UC problem is resolved and updated inside the scheduling interval a finite number of times, e.g. every 3 hours. In [56], a similar two-stage stochastic UC model is described, where commitment decisions are made as a first step and dispatch decisions are made on a second stage based on given scenario realizations.

Both of the stochastic UC models discussed above are described as relatively computational-costly and assume a number of wind power forecast and dispatch data to be available. In both cases, the stochastic models perform better than a deterministic counterpart, but not by much. As the historical VRES data from CAISO is given as net bulk generation from both solar and wind, it's harder to determine specific stochastic probability distributions to forecast VRES generation. Additionally, solar and wind have a different generating nature. Hence, it is justifiable to use a deterministic VRES forecast model in this thesis.

Background

The California power system has a large penetration of VRES, as the state has very suitable conditions for both solar and wind generation. In 2017, 18.03% of the net in-state power generation in California was from wind and solar[57], but more renewable energy sources are scheduled to be installed the coming years, as the state aims to meet its Renewables Portfolio Standard, which requires utilities to source 50% of retail sales from renewables by 2030[58][59].

The ratio between solar to wind generation in California in 2017 was close to 1.9:1[57], and has remained in the same range since. The power output profiles from wind and solar farms are fundamentally different. Both are VRES and have a random generating nature, but while the power output from wind farms tend to flatter and more consistent throughout the day, solar plants only generate power during sun hours. In power systems with a large penetration of solar, such as in California, USA, the power production from solar farms during sun hours causes a rapid decline in power and a rapid increase in power that must be

supplied by other energy sources during sunrise and sunset, respectively[60][61]. Thus, the net power demand curve of a power system resembles the silhouette of a duck and is appropriately often referred to as a *duck curve*. The rapid power ramping during sunset and sunrise is a major challenge with such power systems and will be considered in the robust forecast model.

To illustrate the impact of VRES in power systems, this thesis will consider CAISO load data from one of the summer months, when the power output from both wind and solar is at an annual high. An important notice here is that no day-ahead renewable power forecast is available from CAISO. Hence, it is necessary to establish a VRES generation forecast model. In the months of June and July, power generation from both solar and wind is relatively simililar[59][62][63][64], so this thesis will establish a VRES forecast model for July 2018 based on data from June 2018.

4.4.1 Analysis of June 2018 CAISO VRES Data

The robust VRES forecast model used in this thesis is based on CAISO load data from VRES the entire month of June 2018. The shape of the VRES forecast curve is based on the shape of the average VRES power profile for the entire month of June, while the amplitude of the generating curve is determined by from a Weibull probability distribution regression on the peak renewable generation outputs for each day of the month. The Weibull probability distribution is:

$$f(x|a,b) = \begin{cases} \frac{b}{a}(\frac{x}{a})^{b-1}e^{(\frac{x}{a})^b}, & x \geq 0 \\ 0, & x < 0 \end{cases} \tag{4.7}$$

The parameters a and b in Equation 4.7 are determined using MATLAB, and can be found to be $a = 13312$ and $\mathbf{b} = 11.168$. The Expected value of this function is $\mathbf{E(x)} = 13201$ MW.

4.4.2 Determining uncertainty boundaries

To increase the reliability of the forecast model, a two-side bounded 80%-confidence interval[65] based on the Weibull distribution will be used to determine operation constraints for the day-ahead UC scheduling. The constraints are:

$$\int_0^{\omega_L} \frac{b}{a}(\frac{x}{a})^{b-1}e^{(\frac{x}{a})^b}dx = 10\% \tag{4.8}$$

$$\int_{\omega_U}^{\infty} \frac{b}{a}(\frac{x}{a})^{b-1} e^{(\frac{x}{a})^b} dx = 10\% \tag{4.9}$$

In Equations 4.8 and 4.9, the variables ω_L and ω_U respectively represent lower and upper generating constraints that will be used in the UC model. These parameters are calculated to be $\omega_L = 10883$ MW and $\omega_U = 14345$ MW. The Weibull distribution along with Expected value and 80% confidence interval boundaries is shown in Figure 4.6.

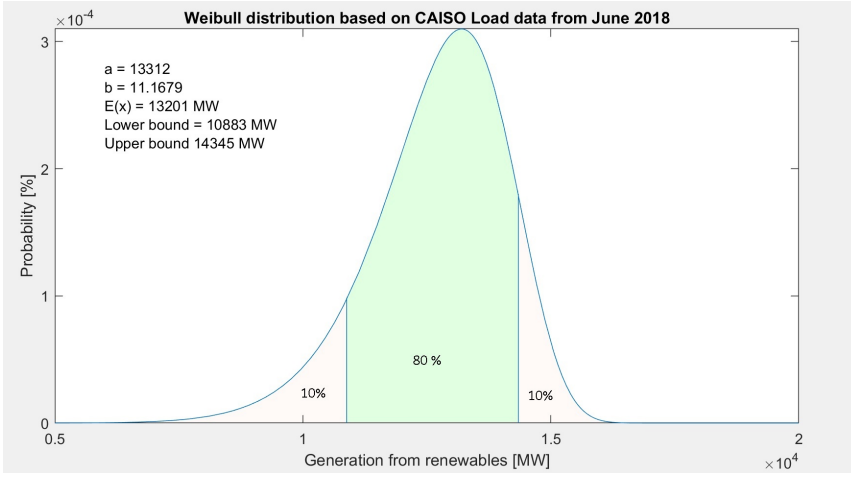

Figure 4.6: VRES Weibull Distribution CAISO June 2018

The RT VRES generation data from CAISO is given as a net sum of wind and solar. Ideally, the data from solar and wind should have been treated separately as they can yield quite different probability distributions due to their different generating nature. As they are combined to one data set, the data from the Weibull distribution regression above will be applied to the net VRES model. The forecast model will be determined by using the hourly average values for VRES generation in June 2018 and scaling them up to a maximum value of the *E(x)* = 13201 MW. Generation constraints and forecast equations are shown below.

$$N_{net}^{forecast}(t) = N^{forecast}(t) - G_{VRES}^{forecast}(t) \tag{4.10}$$

$$\sum_{g} P_{max} U(t,g) + \sum_{e} G_e(t) \geq N^{forecast}(t) - \frac{\omega_L}{E(x)} G_{VRES}^{forecast}(t) + \sum_{e} D_e(t) \tag{4.11}$$

$$\sum_{g} P_{min} U(t,g) + \sum_{e} G_e(t) \leq N^{forecast}(t) - \frac{\omega_U}{E(x)} G_{VRES}^{forecast}(t) + \sum_{e} D_e(t) \tag{4.12}$$

Equation 4.10 states that the forecasted net load is the forecasted load minus the forecasted generation from VRES. Equations 4.11 and 4.12 incorporate the forecast uncertainties of the VRES model into the UC model by ensuring that the committed generating units can compensate for all deviations in VRES power output within the confidence interval boundaries of the VRES. This is shown in the figure below.

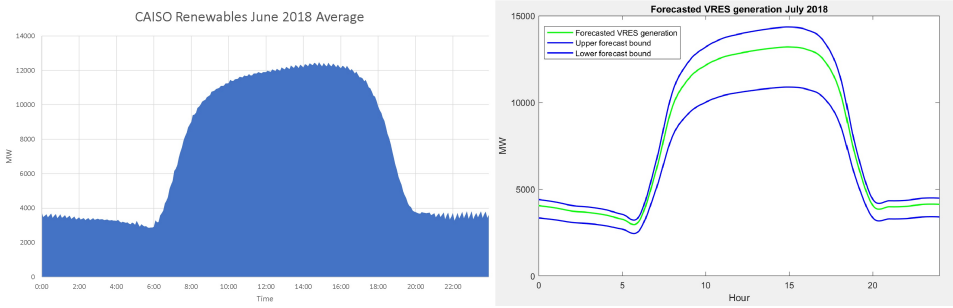

Figure 4.7: VRES uncertainty boundaries for Robust UC

In Figure 4.7, the leftmost plot shows the average CAISO output from VRES output in 5-minute intervals during the month of June 2018, while the rightmost figure shows the derived robust VRES power forecast and confidence boundaries, based on the June 2018 average VRES power and the Weibull distribution described above. The corresponding Bernstein coefficients for the VRES forecast model are shown in Table 4.3:

	H_{00}	H_{01}	H_{10}	H_{11}
t1	4052.684344	-106.8227696	3919.843641	-158.8586382
t2	3919.843641	-158.8586382	3734.967068	-132.6069561
t3	3734.967068	-132.6069561	3654.629728	-111.9112806
t4	3654.629728	-111.9112806	3511.144507	-193.5072625
t5	3511.144507	-193.5072625	3267.615203	-181.8018892
t6	3267.615203	-181.8018892	3147.540728	1365.051511
t7	3147.540728	1365.051511	5997.718224	3290.684319
t8	5997.718224	3290.684319	9728.909366	2701.783569
t9	9728.909366	2701.783569	11401.28536	1207.091903
t10	11401.28536	1207.091903	12143.09317	598.358547
t11	12143.09317	598.358547	12598.00246	343.1238702
t12	12598.00246	343.1238702	12829.34091	202.4256422
t13	12829.34091	202.4256422	13002.85374	151.8821638
t14	13002.85374	151.8821638	13133.10524	99.07312921
t15	13133.10524	99.07312921	13201	-30.89067804
t16	13201	-30.89067804	13071.32388	-343.0159865
t17	13071.32388	-343.0159865	12514.96803	-1179.114082
t18	12514.96803	-1179.114082	10713.09572	-2888.368299
t19	10713.09572	-2888.368299	6738.231428	-3322.024512
t20	6738.231428	-3322.024512	4069.046694	-1373.07086
t21	4069.046694	-1373.07086	3992.089708	-28.12166499
t22	3992.089708	-28.12166499	4012.803364	64.17277643
t23	4012.803364	64.17277643	4120.435261	53.81594841
t24	4120.435261	53.81594841	4120.435261	-53.81594841

Table 4.3: VRES Forecast model for CAISO June 2018

4.5 Net Robust Optimization model

In case studies 1 and 2 in this thesis, the only uncertainty variable is the day-ahead load forecast profile. In case 3, VRES input is also included. Hence, the day-ahead load forecast model needs to account for the uncertainty sets of both forecasts. To determine uncertainty constraints, the combined standard uncertainty model in [66] will be used to combine the robust generating constraints with the VRES power forecast uncertainty to form new generating constraints for the Robust optimization model.

$$\Delta N_{k,lo}^{R,vres} = \sqrt{(\Delta N_{k}^{R,vres})^2 + (1 - \frac{\omega_L}{E(x)})G_{VRES}^{forecast})^2} \tag{4.13}$$

$$\Delta N_{k,up}^{R,vres} = \sqrt{(\Delta N_{k}^{R,vres})^2 + ((\frac{\omega_U}{E(x)} - 1)G_{VRES}^{forecast})^2} \tag{4.14}$$

In Equation 4.13 and 4.12, the parameter $N_{k}^{R,vres}$ is the robust uncertainty boundary defined in Chapter 4, while the variables ω_L, ω_U and *E(x)* are the VRES forecast variables described in this section. $\Delta N_{k,up}^{R,vres}$ and $\Delta N_{k,lo}^{R,vres}$ represents the net upper and lower robust generating constraints that will be used for the robust formulation of the UC model.

4.5.1 Applicability

As details of the probability distributions of forecasting errors are assumed to be unknown, a robust optimization model is preferred over a stochastic optimization model in this thesis. Data from CAISO has been used to provide empirical forecast error data. An important note for the model is that the sum of uncertainty bounds and forecasted load will be capped at 2850 MW, as this is the maximum possible load in the IEEE 24-bus RTS.

The robust load uncertainty set is defined in terms of relative functions, and can, in theory, be applied to any load forecast set. The robust VRES uncertainty set, however, is specifically designed for the California Power System, and only for summer months. To justly apply the robust VRES uncertainty set, it will hence be applied to the case study on July 2nd, 2018, such that the forecast set is based on as recent empirical VRES data as possible.

Chapter 5

Case Studies

The simulation case studies will not consider any hour-ahead markets, where the DA load forecasts are updated and further market bids are submitted. This is an important market aspect of power systems operations in many market structures and with many ISO[67], but will not be included in the case studies. This is has been done to avoid complicating the UC model further, and is beyond the scope of this thesis. The main goal of these computations is to compare the Bernstein UC model with the current UC model.

The proposed UC model will be assessed through three different case studies. Each case will be simulated using the Bernstein UC model, and compared to the traditional UC model simulated on the same case. For each of the three cases, the UC simulation will be solved using the four submodels, that aim to highlight possible UC scheduling scenarios and their impact on scheduling costs. ES systems exist in a wide number of technologies and can provide an array of enhancements in power system operations[68][69]. A higher penetration of renewable generation introduces greater uncertainties, and introduce variations of greater magnitude and frequency[70] than before. It is thus expedient to design UC models that investigate this issue.

The UC models are simulated on three different load data sets from CAISO. One Case is selected to represent large load forecasting errors, another case is selected to represent low forecasting errors, and a final set is selected to show the impact of VRES penetration. The data set that is used for the large forecast error test is CAISO load data from May 4th, 2018, the low forecast error data set is CAISO load data from August 4th, 2018, while the data set with VRES penetration is from July 2nd, 2018. The July data set is selected because power

both solar and wind is at an annual high during summer, and hence the impact of VRES will be as large as possible for this case.

5.1 Case Solver

The cases were solved using GAMS CPLEX solver with a duality gap of 0.0, on a computer with a 2x2.60 GHz Xeon processor and 384 GB of RAM. The number of binary variables is the same for both the Bernstein and traditional UC model, while the number of floating variables, equations and constraints are higher for the Bernstein model, and hence the Bernstein models require slightly more computation time. All models were solved in under 2s. Simulation results are presented in Chapter 6. Code used to solve the UC problem is listen in Appendix C.

5.2 Case 1: May 4th, 2018 Load Profile

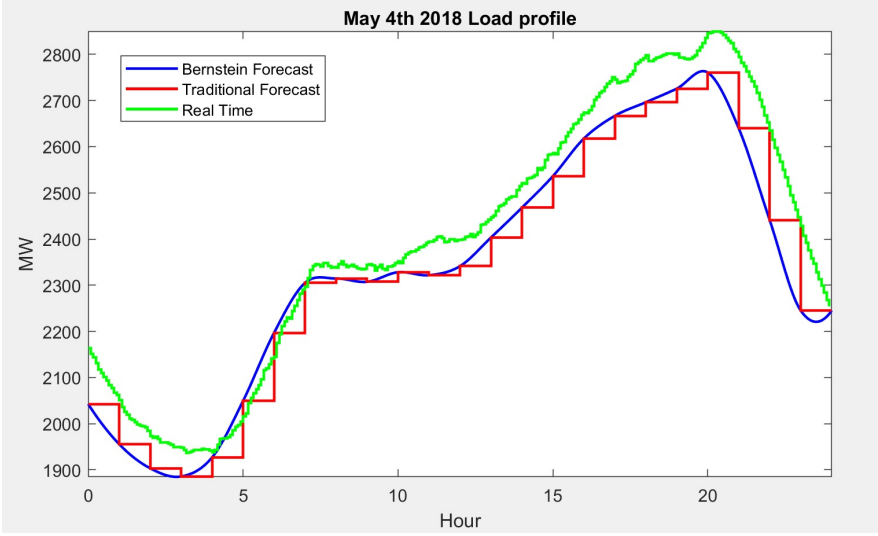

Figure 5.1: CAISO May 5th 2018 Load Profile scaled down to a maximum value of 2850 MW

Figure 5.1 shows the CAISO Load Data from May 5th, 2018 load profile. The data has moderate DA forecast errors throughout the entire scheduling interval but has significant forecast errors from hour 20 to 24. These errors make up main challenges for the RT UC operation and must be countered during the RT operation of the grid. For Case 1, May 4th, the Bernstein model forecasts a 0.15% larger energy demand than the traditional model.

5.3 Case 2: August 4th, 2018 Load Profile

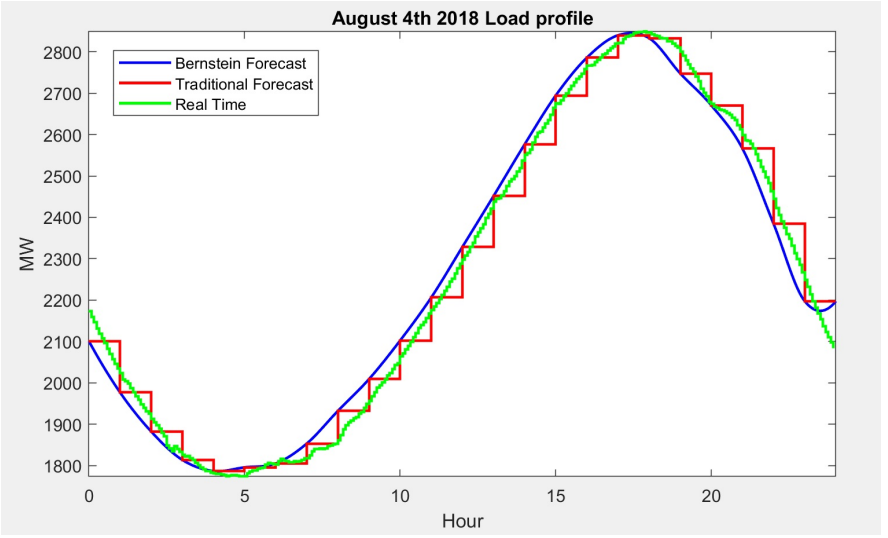

Figure 5.2: CAISO August 4th 2018 Load Profile scaled down to a maximum value of 2850 MW

Figure 5.2 shows the CAISO Load Data from August 4th, 2018 load profile. The data has low DA forecast errors throughout the entire scheduling interval. Hence, RT operation costs are expected to be low. For Case 2, August 4th, the Bernstein UC model forecasts a 0.05% larger energy demand than the traditional model.

5.4 Case 3: July 2nd, 2018 Load Profile with VRES penetration

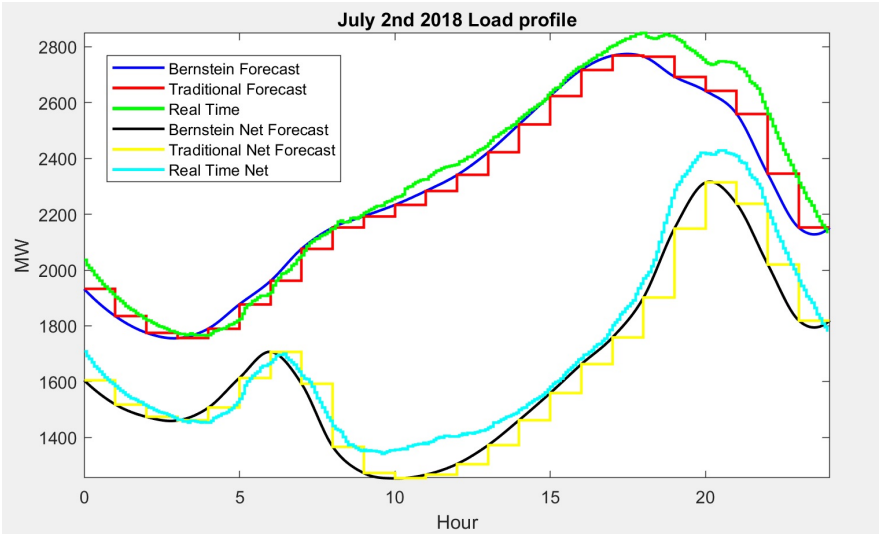

Figure 5.3: CAISO August 4th 2018 Load Profile scaled down to a maximum value of 2850 MW

Figure 5.3 shows the CAISO Load Data from July 2nd, 2018 load profile. The data has moderate DA forecast load errors and low VRES forecast errors throughout the entire scheduling interval. The case will be simulated on the net load demand curve which is the total system demand minus power from VRES. For reference, the case will also be solved without VRES penetration. For Case 3, July 2nd, the Bernstein model forecasts a 0.22% larger energy demand than the traditional model with VRES penetration, and a 0.17% larger energy demand without VRES generation.

Chapter 6

Results and discussion

6.1 Case 1: May 4th, 2018 Load Profile

6.1.1 Standard UC model

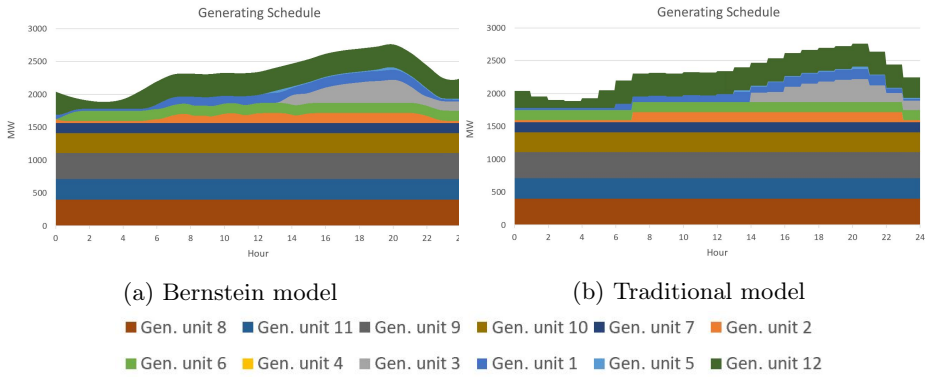

(a) Bernstein model (b) Traditional model

Figure 6.1: Standard UC DA generating schedules May 4th

Figure 6.1a and Figure 6.1b respectively show the generating schedule of the standard UC case, using the Bernstein and traditional model. The forecasted load ramps consistently from time t = 12 to t = 20. The Bernstein model shuts down generating unit 4 and starts up generating unit 6 at time t = 0.

Generating unit 5 is committed from time t = 12, and unit 3 is committed from time t = 13. The traditional model also shuts down unit 4 and starts up unit 6 at time t = 0. Generating unit 5 is committed from time t = 13 and generating unit 3 is committed from time t = 14.

Model	DA cost	RT operation	Net costs
Bernstein	$473,129.67	$20,610.87	$493,740.54
Standard	$471,106.12	$112,607.51	$583,713.63

Table 6.1: Standard UC costs May 4th 2018

Table 6.1 shows that the DA costs from both models are in the same range. The RT operation costs are much higher for the traditional model than the Bernstein model. Both models suffer from generating capacity scarcity between hours 18-21, however, the traditional model suffers from both ramping and generating scarcity during hours 11-14 and relies heavily on auxiliary generation. Hence the net operation costs are $89,973.09 higher for the traditional model than the Bernstein model.

6.1.2 Robust UC model

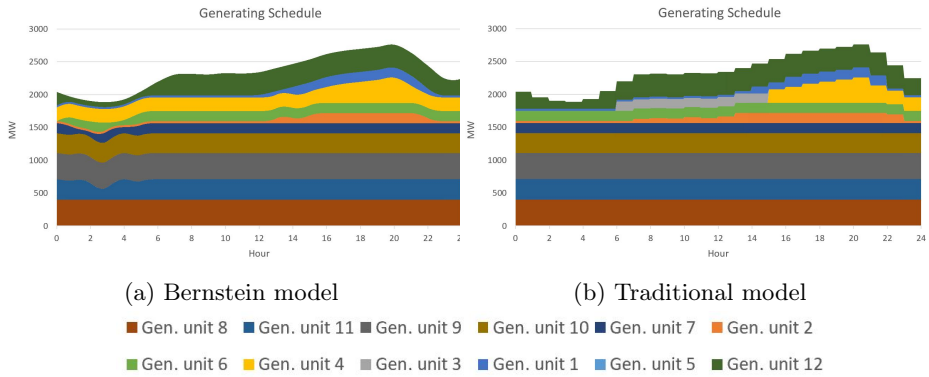

(a) Bernstein model (b) Traditional model

Figure 6.2: Robust UC DA generating schedules May 4th

Figure 6.2a and Figure 6.2b respectively show the generating schedule of the robust UC case, using the Bernstein and traditional model. The Bernstein

model starts ups generating unit 6 at time t = 0. The traditional model shuts down unit 4 and starts up unit 6 at time t = 0. Generating unit 3 is committed from time t = 6 and shut down at time t = 15. Generating unit 4 is committed again from time t = 15.

Model	DA cost	RT operation	Net costs
Bernstein	$493,876.44	$12,763.43	$506,639.87
Standard	$484,495.56	$17,071.09	$501,566.65

Table 6.2: Robust UC costs May 4th 2018

As seen in Table 6.2, the Bernstein model has much higher DA scheduling costs than the traditional model, but does in return have lower RT operating costs. Neither of the models need to commit any auxiliary generation, unlike the standard model without the added robust constraints. The net operation costs are $5,073.22 higher for the Bernstein model.

6.1.3 Standard UC model with ESs units

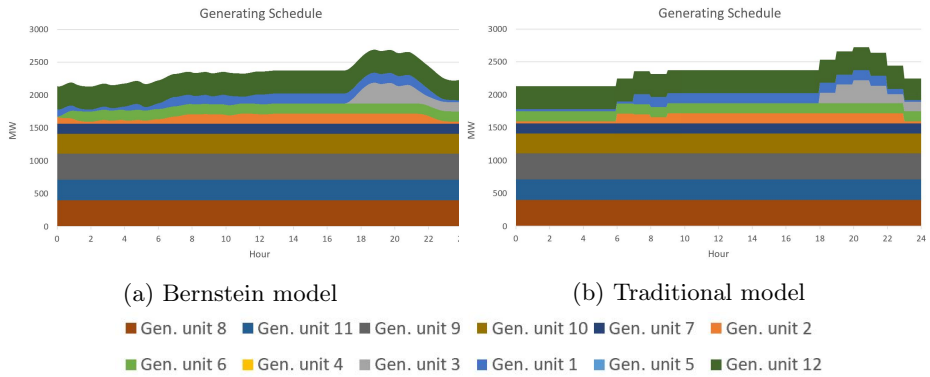

(a) Bernstein model (b) Traditional model

Figure 6.3: Standard UC with ES DA generating schedules May 4th

Figure 6.3a and Figure 6.3b respectively show the generating schedule of the standard UC case, using the Bernstein and traditional model. The Bernstein model shuts down generating unit 4 and starts up generating unit 6 at time t = 0. Generating unit 3 is committed from time t = 17. The traditional model

also shuts down unit 4 and starts up unit 6 at time t = 0. Generating unit 3 is committed from time t = 18 and runs through the rest of the scheduling period.

Model	DA cost	RT operation	Net costs
Bernstein	$463,630.88	$30,420.11	$494,050.99
Traditional	$461,655.54	$388,646.39	$850,301.93

Table 6.3: Standard with ESS UC costs May 4th 2018

Both models need auxiliary generation in the time span from t = 11 to t = 22, but while the Bernstein model only needs moderate inputs from period t = 10 to t = 16, the traditional model relies heavily on auxiliary generation input from t = 9 to t = 18. As seen in Table 6.3, this causes high RT operation costs, with net operation costs for the traditional model $356,250.94 higher than the Bernstein model. While the ES units contribute to peak load shaving[23] by discharging power from time t = 12, the heavy price paid is due to less generating units being committed and hence less available generating capacity during the peak load period. Figures showing ES unit power flow and SOC can be found in Appendix A.

6.1.4 Robust UC model with ESS units

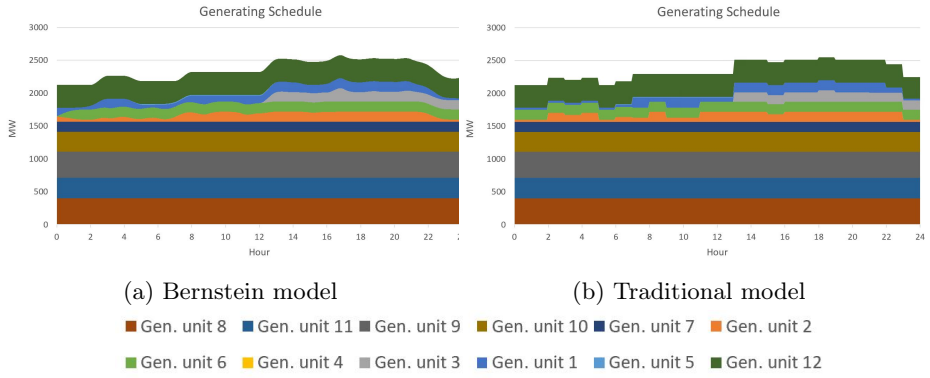

(a) Bernstein model (b) Traditional model

Figure 6.4: Robust UC with ES DA generating schedules May 4th

Figure 6.4a and Figure 6.4b respectively show the generating schedule of the robust UC case, using the Bernstein and traditional model. The Bernstein

model shuts down generating unit 4 and starts up generating unit 6 at time t = 0. Generating unit 5 is committed from time t = 4 and shuts down again at time t = 13. Additionally, generating unit 3 is committed from time t = 12. The traditional model also shuts down unit 4 and starts up unit 6 at time t = 0. Generating unit 5 is committed from time t = 6 and shut down at time t = 13. Generating unit 3 is committed from time t = 13.

Model	DA cost	RT operation	Net costs
Bernstein	$468.192,48	$17,104.26	$485,296.74
Traditional	$465,516.33	$23,628.40	$489,144.73

Table 6.4: Robust with ES UC costs May 4th 2018

Table 6.4 shows that the models have similar DA scheduling and RT operation costs. The traditional model has lower DA scheduling costs, but the Bernstein model has lower RT operation costs. The Bernstein model does not commit any auxiliary generation, but the traditional model needs auxiliary input at time t = 5 due to ramping scarcity. The net operation costs are $3,847.99 lower for the Bernstein model. Figures showing ES unit power flow and SOC can be found in Appendix A.

6.2 Case 2: August 4th, 2018 Load Profile

6.2.1 Standard UC model

Figure 6.5a and Figure 6.5b respectively show the generating schedule of the standard UC case, using the Bernstein and traditional UC model. The forecasted load profile ramps consistently from time t = 5 to t = 17 and hence extra generating capacity is needed. The Bernstein starts ups generating unit 6 at time t = 0. The traditional shuts down unit 4 and starts up unit 6 at time t = 0. Generating unit 4 is committed again from time t = 13. The lo

Model	DA cost	RT operation	Net costs
Bernstein	$480,030.38	$3,087.33	$483,117.71
Standard	$458,591.40	$10,143.96	$468,735.17

Table 6.5: Standard UC costs August 4th 2018

As seen in Table 6.5, the DA costs are much lower for the traditional model

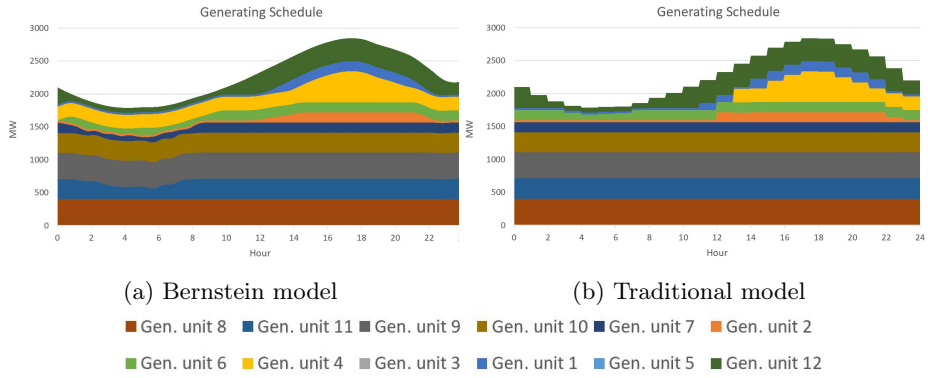

(a) Bernstein model (b) Traditional model

Figure 6.5: Standard UC DA generating schedules August 4th

than the Bernstein model. This is due to the Bernstein model scheduling for ramping between hours t = 10 and t = 16. The RT operation costs are more than three times as large for the traditional model as the Bernstein model. While the Bernstein model does not commit any auxiliary generation at all, the traditional model needs a small amount of auxiliary input around time t = 13. The net operation costs are $14,382.54 higher for the Bernstein model than the traditional model.

6.2.2 Robust UC model

Figure 6.6a and Figure 6.6b respectively show the generating schedule of the robust UC case, using the Bernstein and traditional model. The Bernstein starts ups generating unit 6 at time t = 0. The traditional model shuts down unit 4 and starts up unit 6 at time t = 0. Generating unit 4 is committed again from time t = 11.

Model	DA cost	RT operation	Net costs
Bernstein	$480,030.38	$3,087.33	$483,117.71
Standard	$462,080.83	$5,330.62	$467,411.45

Table 6.6: Robust UC costs August 4th 2018

Table 6.6 shows that the Bernstein model has the exact same DA schedule as in the standard submodel, and has DA scheduling significantly higher DA

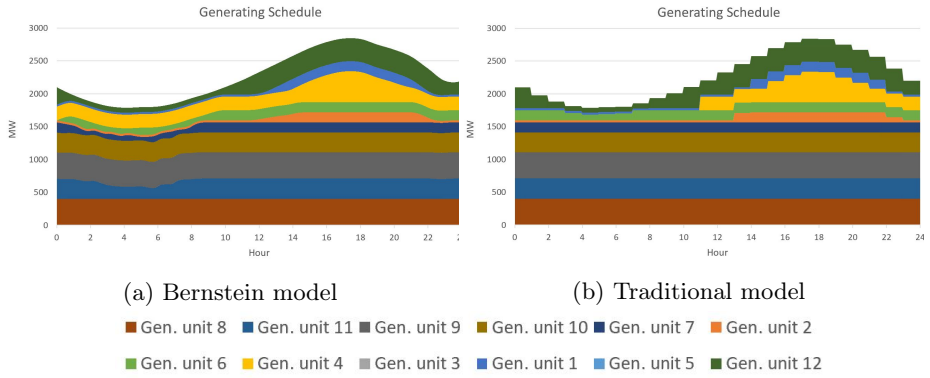

(a) Bernstein model (b) Traditional model

Figure 6.6: Robust UC DA generating schedules August 4th

scheduling costs than the traditional model. The traditional model has much higher RT operation costs, but the robust constraints have reduced the RT costs of the traditional model to about 50% of the scheduling costs for the standard model. Neither of the models need to commit any auxiliary generation. The net operation costs are $15,706.26 higher for the Bernstein model.

6.2.3 Standard UC model with ES units

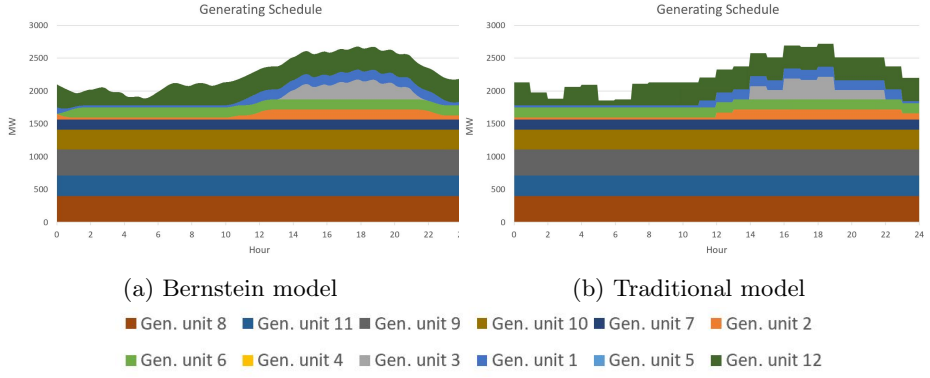

(a) Bernstein model (b) Traditional model

Figure 6.7: Standard UC with ES DA generating schedules August 4th

Figure 6.7a and Figure 6.7b respectively show the generating schedule of the standard UC case, using the Bernstein and traditional model. The Bernstein model shuts down generating unit 4 and starts up generating unit 6 at time t = 0. Generating unit 3 is committed at time t = 13 and shut down at time t = 22. The traditional model also shuts down unit 4 and starts up unit 6 at time t = 0. Generating unit 3 is committed from time t = 14 and shut down at time t = t = 22.

Model	DA cost	RT operation	Net costs
Bernstein	$446.264,99	$5,394.53	$451,659.52
Traditional	$445,538.01	$41,987.57	$487,525.58

Table 6.7: Standard with ES UC costs August 4th 2018

As seen in Table 6.7, the two models have very similar DA scheduling costs, however, the Bernstein has significantly lower RT operation costs at $5,394.53 compared to $41,987.57 for the traditional model. Both models need auxiliary generation around time t = 22. The traditional model also needs auxiliary generation at certain other points in the scheduling time frame, particularly between t = 13 and t = 14. This is the reason why the traditional model has much higher RT operation costs. The net operation costs are $35,866.06 higher for the traditional model than the Bernstein model. Figures showing ES unit power flow and SOC can be found in Appendix A.

6.2.4 Robust UC model with ESS units

Figure 6.8a and Figure 6.8b respectively show the generating schedule of the robust UC case, using the Bernstein and traditional model. The Bernstein model shuts down generating unit 4 and starts up generating unit 6 at time t = 0. Generating unit 3 is committed from time t = 11 and runs through the rest of the period. The traditional model also shuts down unit 4 and starts up unit 6 at time t = 0. Generating unit 3 is committed from time t = 12.

Model	DA cost	RT operation	Net costs
Bernstein	$449.592,25	$4,568.33	$454,160.58
Traditional	$447,973.62	$18,352.01	$466,325.63

Table 6.8: Robust with ES UC costs August 4th 2018

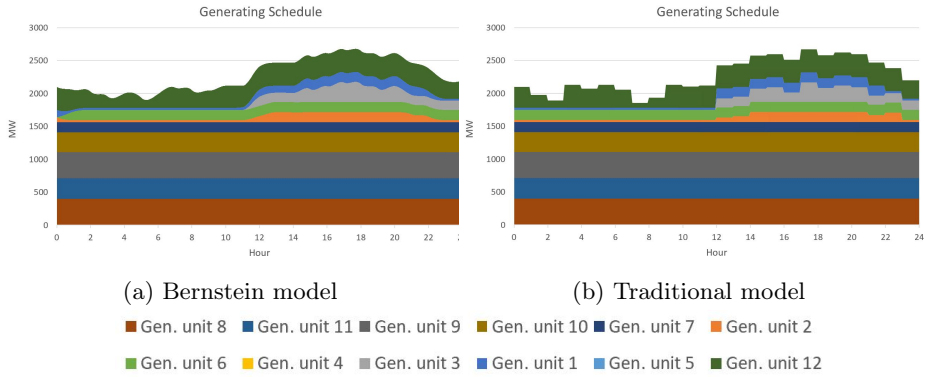

(a) Bernstein model (b) Traditional model

Figure 6.8: Robust UC with ES DA generating schedules August 4th

Table 6.8 shows that the models have DA scheduling costs in the same range, but the Bernstein model has much lower RT operation costs. However, the robust constraints have reduced the RT costs of the traditional model by about 50%. The Bernstein model commits no auxiliary generation, but the traditional model needs auxiliary support at hours 3 and 7. The net operation costs are \$12,165.05 lower for the Bernstein model. Figures showing ES unit power flow and SOC can be found in Appendix A.

6.3 Case 3: July 2nd, 2018 Load Profile with VRES penetration

6.3.1 Standard UC model

Figure 6.9a and Figure 6.9b respectively show the generating schedule of the standard UC case, using the Bernstein and traditional model. The Bernstein model shuts down generating unit 4 at time t = 0. Generating unit 11 is shut down at time t = 8 and started up again at time t = 16. Unit 6 is committed from time t = 12. The traditional model also shuts down unit 4 at time t = 0. Generating unit 11 is shut down from time t = 8 and started up again at time t = 16. Generating unit 6 is committed from time t = 14.

Table 6.9 shows that the DA costs from both models are in the same range. The RT operation costs are more than twice as large for the traditional model as

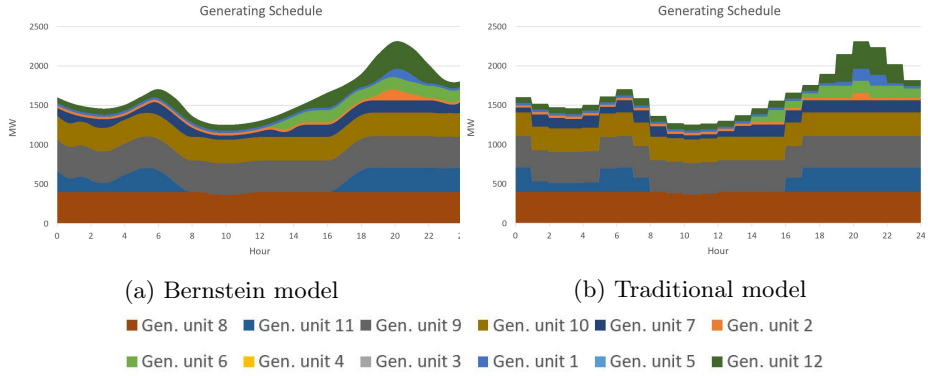

(a) Bernstein model (b) Traditional model

Figure 6.9: Standard UC DA generating schedules July 2nd

Model	DA cost	RT operation	Net costs
Bernstein	$257,121.14	$25,294.65	$282,415.79
Standard	$255,959.33	$57,674.80	$313,634.13

Table 6.9: Standard UC costs July 2nd 2018 (VRES penetration)

Model	DA cost	RT operation	Net costs
Bernstein	$454,102.85	$21,680.10	$475,782.95
Standard	$452,302.40	$185,892.22	$638,194.62

Table 6.10: Standard UC costs July 2nd 2018 (no VRES)

for the Bernstein model. Both models need auxiliary generation between time t = 20 and t = 22. The net operation costs are $31,218.34 lower for the Bernstein model than the traditional model. Table 6.10 shows UC costs for the same load profile without VRES penetration for reference.

6.3.2 Robust UC model

Figure 6.10a and Figure 6.10b respectively show the generating schedule of the robust UC case, using the Bernstein and traditional model. The Bernstein model shuts down generating unit 4 at time t = 0. Generating unit 11 is shut down at time t = 8 and started up again at time t = 16. Generating unit 6 is

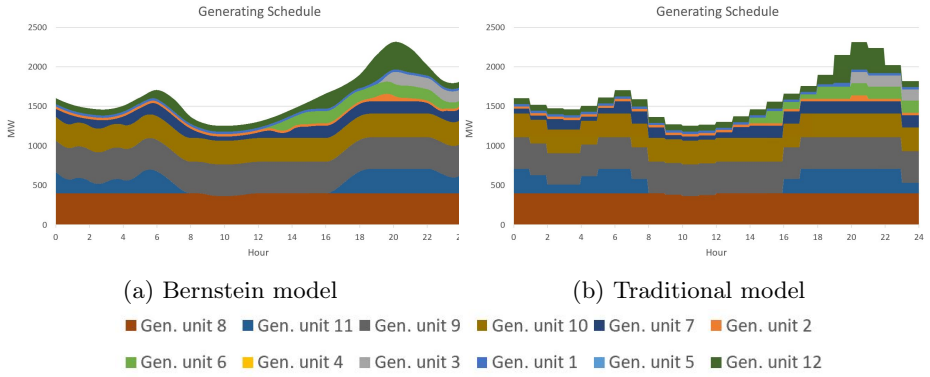

(a) Bernstein model (b) Traditional model

Figure 6.10: Robust UC DA generating schedules July 2nd

committed from time t = 12, and unit 3 is committed from time t = 19. The traditional model also shuts down unit 4 at time t = 0. Generating unit 11 is shut down at time t = 8 and started up again at time t = 16. Generating unit 6 is committed from time t = 14, and unit 3 is committed from time t = 20.

Model	DA cost	RT operation	Net costs
Bernstein	$264,531.34	$20,305.59	$284,836.93
Standard	$262,630.74	$32,588.52	$295,219.26

Table 6.11: Robust UC costs July 2nd 2018 (VRES penetration)

Model	DA cost	RT operation	Net costs
Bernstein	$477,307.02	$10,548.02	$487,855.04
Standard	$459,127.23	$14,354.05	$473,481.28

Table 6.12: Standard UC costs July 2nd 2018 (no VRES)

Table 6.11 shows that the models have DA scheduling costs in the same range, but the RT operation costs for the traditional model are about 50% higher than for the Bernstein model. While the Bernstein model doesn't need to commit any auxiliary generation, the traditional model needs auxiliary generation due to ramping scarcity at time t = 20. The net operation costs are

$10,382.33 lower for the Bernstein model. Table 6.12 shows UC costs for the same load profile without VRES penetration for reference.

6.3.3 Standard UC model with ESs units

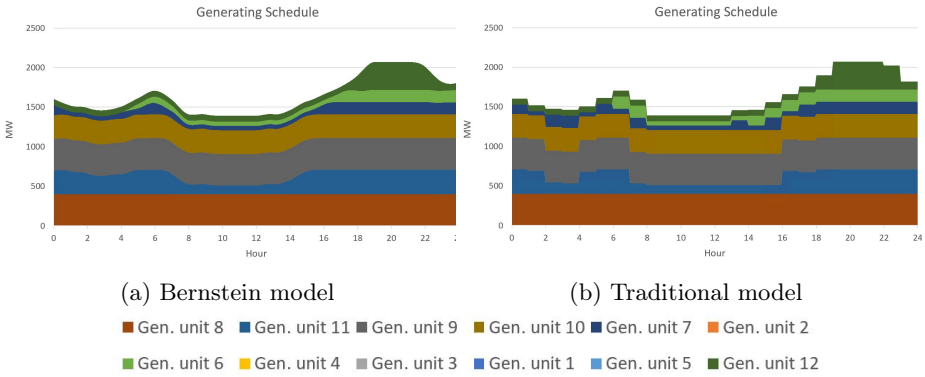

(a) Bernstein model (b) Traditional model

Figure 6.11: Standard UC with ES DA generating schedules July 2nd

Figure 6.11a and Figure 6.11b respectively show the generating schedule of the standard UC case, using the Bernstein and traditional model. The Bernstein model shuts down generating unit 1, unit 2 and unit 4 at time t = 0. Generating unit 6 is committed from time t = 4. The traditional model also shuts down generating unit 1, unit 2 and unit 4 at time t = 0. Generating unit 6 is committed from time t = 6.

Model	DA cost	RT operation	Net costs
Bernstein	$254.256,56	$38,683.79	$292,940.35
Traditional	$253,276.61	$269,932.70	$523,209.31

Table 6.13: Standard with ES UC costs July 2nd 2018 (VRES penetration)

From Table 6.13 it can be seen that the two models have very similar DA scheduling costs, however, the Bernstein has significantly lower RT operation costs at $38,683.79 compared to $269,932.70 for the traditional model. Both models suffer from significant generating scarcity between time t = 18 to time t = 23. The traditional model also has significant ramping scarcity between

Model	DA cost	RT operation	Net costs
Bernstein	$443.444,17	$21,334.54	$464,778.71
Traditional	$442,222.40	$122,875.17	$565,097.57

Table 6.14: Standard with ES UC costs July 2nd 2018 (no VRES)

t = 19 and t = 20. This is the reason why the traditional model has much higher RT operation costs. The net operation costs are $239,268.96 higher for the traditional model than the Bernstein model. Table 6.14 shows UC costs for the same load profile without VRES penetration for reference. Figures showing ES unit power flow and SOC can be found in Appendix A.

6.3.4 Robust UC model with ESS units

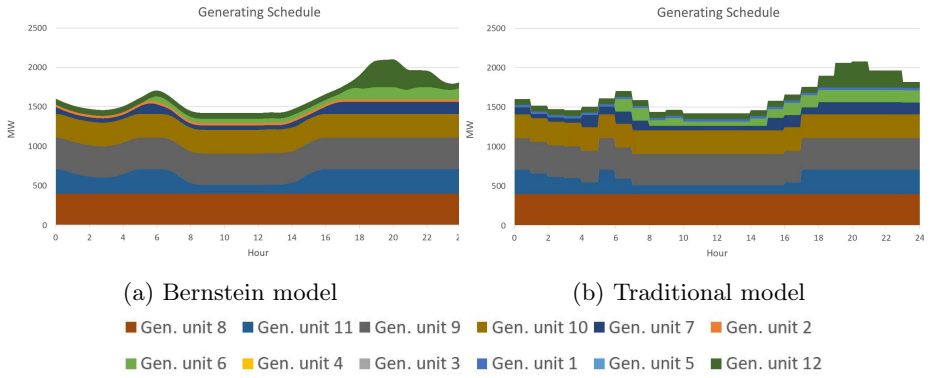

(a) Bernstein model (b) Traditional model

Figure 6.12: Robust UC with ES DA generating schedules July 2nd

Figure 6.12a and Figure 6.12b respectively show the generating schedule of the robust UC case, using the Bernstein and traditional model. The Bernstein model shuts down generating unit 1 and unit 4 at time t = 0. Generating unit 6 is committed from time t = 5. The traditional model shuts down unit 2 and unit 4 at time t = 0. Generating unit 6 is committed from time t = 6.

Table 6.15 shows that the models have DA scheduling costs in the same range, but again the Bernstein model has much lower RT operation costs, at below 50% of the traditional model. The Bernstein model does not commit

Model	DA cost	RT operation	Net costs
Bernstein	$255.047,25	$25,042.53	$280,089.78
Traditional	$254,155.21	$56,976.97	$311,132.18

Table 6.15: Robust with ES UC costs July 2nd 2018 (VRES penetration)

Model	DA cost	RT operation	Net costs
Bernstein	$446.166,05	$14,747.77	$460,913.82
Traditional	$444,739.79	$21,872.08	$466,611.87

Table 6.16: Robust with ES UC costs July 2nd 2018 (no VRES)

any auxiliary generation, but the traditional model needs auxiliary generation between t = 19 and t = 20 and at time t = 22. The net operation costs are $31,042.40 lower for the Bernstein model. Table 6.16 shows UC costs for the same load profile without VRES penetration for reference. Figures showing ES unit power flow and SOC can be found in Appendix A.

6.4 Discussion and interpretation

To assess the performance of the proposed Bernstein DA UC model, the results from the three different case studies will be interpreted in terms of several aspects. The DA scheduling and RT operation costs for the UC models are summed up in Table 6.17, Table 6.18, Table 6.19 and Table 6.20 below. The simulations in this thesis are based on the IEEE 24-bus RTS, with 12 generating units. All the unit data used for the simulations are given in bulk generating bus quantities, and economic costs are calculated based on this. Hence, it does not perfectly reflect how the UC models perform in a real-life power system in terms of costs. Such systems may have thousands of generating units and corresponding energy bids that must be handled in the UC problem DA scheduling. However, the results from the case studies in this thesis can be used to highlight some crucial aspects of power system operation.

The RT operational costs for a given UC scheduling simulation reflect generating, and perhaps more importantly, ramping scarcities from the day-ahead UC scheduling. A poor UC scheduling may lead to the need for expensive auxiliary generating during the RT operation, leading to high RT operation costs. For most cases simulated with the standard submodel, the DA scheduling costs

for the Bernstein model were less than 0.5% larger than for the traditional model, i.e. almost negligible. The one exception was in Case 2, where the DA scheduling costs were close to 5% larger for the Bernstein model due to steep and protracted forecast ramping between hour t = 6 and t = 16. An important note here, however, is that this issue was significantly reduced with ES units present in the system, as their fast-ramping capabilities relieved much of the ramping stress from the generating units.

As stated earlier in this thesis, the hour-ahead market, as well as the 5-minute RT market in power systems with VRES penetration[71], is not implemented into the UC simulations in this paper, and hence the worst case RT costs for certain of the submodels in some of the case studies would likely be lower in real life operation. Still, RT costs from the UC simulations in this thesis reflect the forecasting and scheduling errors of the respective models and provide an excellent basis to assess the performance of the proposed Bernstein UC model.

6.4.1 Summary of Case simulations

Submodel	Model	DA cost	RT operation	Net costs	Diff.
Standard	Bernstein	\$473,129.67	\$20,610.87	\$493,740.54	
	Traditional	\$471,106.12	\$112,607.51	\$583,713.63	+\$89,973.09
Robust	Bernstein	\$493,876.44	\$12,763.43	\$506,639.87	+\$5,073.22
	Traditional	\$484,495.56	\$17,071.09	\$501,566.65	
Std. w/ES	Bernstein	\$463,630.88	\$30,420.11	\$494,050.99	
	Traditional	\$461,655.54	\$388,646.39	\$850,301.93	+\$356,250.94
Rob. w/ES	Bernstein	\$468.192,48	\$17,104.26	\$485,296.74	
	Traditional	\$465,516.33	\$23,628.40	\$489,144.73	+\$3,847.99

Table 6.17: Summary UC costs Case 1: May 4th

Submodel	Model	DA cost	RT operation	Net costs	Diff.
Standard	Bernstein	$480,030.38	$3,087.33	$483,117.71	+$14,382.54
	Traditional	$458,591.40	$10,143.96	$468,735.17	
Robust	Bernstein	$480,030.38	$3,087.33	$483,117.71	+$15,706.26
	Traditional	$462,080.83	$5,330.62	$467,411.45	
Std. w/ES	Bernstein	$446.264,99	$5,394.53	$451,659.52	
	Traditional	$445,538.01	$41,987.57	$487,525.58	+$35,866.06
Rob. w/ES	Bernstein	$449.592,25	$4,568.33	$454,160.58	
	Traditional	$447,973.62	$18,352.01	$466,325.64	+$12,165.05

Table 6.18: Summary UC costs Case 2: August 4th

Submodel	Model	DA cost	RT operation	Net costs	Diff.
Standard	Bernstein	$257,121.14	$25,294.65	$282,415.79	
	Traditional	$255,959.33	$57,674.80	$313,634.13	+$31,218.34
Robust	Bernstein	$264,531.34	$20,305.59	$284,836.93	
	Traditional	$262,630.74	$32,588.52	$295,219.26	+$10,382.33
Std. w/ES	Bernstein	$254.256,56	$38,683.79	$292,940.35	
	Traditional	$253,276.61	$269,932.70	$523,209.31	+$239,268.96
Rob. w/ES	Bernstein	$255.047,25	$25,042.53	$280,089.78	
	Traditional	$254,155.21	$56,976.97	$311,132.18	+$31,042.40

Table 6.19: Summary UC costs Case 3: July 2nd (VRES penetration)

Submodel	Model	DA cost	RT operation	Net costs	Diff.
Standard	Bernstein	$454,102.85	$21,680.10	$475,782.95	
	Traditional	$452,302.40	$185,892.22	$638,194.62	+$162,411.67
Robust	Bernstein	$477,307.02	$10,548.02	$487,855.04	+$14,373.76
	Traditional	$459,127.23	$14,354.05	$473,481.28	
Std. w/ES	Bernstein	$443.444,17	$21,334.54	$464,778.71	
	Traditional	$442,222.40	$122,875.17	$565,097.57	+$100,318.86
Rob. w/ES	Bernstein	$446.166,05	$14,747.77	$460,913.82	
	Traditional	$444,739.79	$21,872.08	$466,611.87	+$5,698.05

Table 6.20: Summary UC costs Case 3: July 2nd (no VRES)

Chapter 7

Conclusion

7.1 Bernstein vs Traditional UC problem formulation

The Bernstein UC model and the traditional UC model have similar DA commitment schedules for most cases and submodel simulations. A noticeable trend is that the Bernstein model tends to start up and commit generating units one time-step ahead of the traditional UC model in periods with significant ramp-up. The advantage of this becomes very clear in e.g. Case 1 in both the standard and standard with ES submodel, where RT operating costs for the traditional model respectively were 546% and 1277% higher than their Bernstein UC model counterparts.

While it is obviously a goal to minimize net UC operation costs, it is also a goal to minimize the need for auxiliary generation during RT operation. In every single case study, the traditional model had a higher need for auxiliary generation than the Bernstein model. In several simulations, where the traditional UC model needed auxiliary generation, the Bernstein UC model didn't need any at all. This is one of the key takeaways from this thesis. The Bernstein UC model has a robust nature that captures sub-hourly variations much better than the traditional UC model.

7.2 Submodels

The Bernstein UC model performs significantly more consistent than the traditional model without added robust constraints, as the Bernstein UC model has a robust nature itself. The robust constraint submodels had a very positive effect on the traditional UC model, lowering the net operation costs for every case study, perhaps a little surprisingly also for Case 2, where forecast errors were very low. For the Bernstein UC model, the standard UC submodel costs were lower or equal to the net costs for the robust submodel for all cases simulated. An important issue to keep in mind, however, is that the robust submodel reduced the need for auxiliary generation. Nevertheless, the robust UC constraints benefited the traditional model more than the Bernstein model.

Integrating ES units in power systems effectively lower the DA scheduling costs of the UC problem. However, charging ES units will mean occupying some of the spinning reserves in the system, and the power provided from discharging ES units may lead to generating units being shut down, hence also reducing spinning reserves. Hence, the standard with ES UC model is particularly vulnerable to load forecast errors, as can be seen from high RT costs in several cases, particularly in Case 1 and Case 3. Added robust constraints for ES scheduling had a positive effect on net UC operation costs for both the traditional and the Bernstein UC model. For every case simulation, except in case 2, the robust with ES submodel on the Bernstein formulation gave the lowest net costs. Case 2 had very low forecast errors, and here, the robust with ES Bernstein submodel was second best, only beaten by the standard with ES Bernstein submodel at 0.55% lower costs.

7.3 Concluding remarks

The results of the simulations in this thesis show that the Bernstein UC model performs much more consistent than the traditional UC model, and its main advantages are shown in the case studies where day-ahead forecast errors are large, when there are large sub-hourly load variations and when there is large load ramping. The robust nature of the Bernstein UC model yield lower RT operational costs and fewer ramping scarcity events than the traditional UC model.

An important takeaway from the simulations in the thesis is that the continuous time Bernstein UC model, schedules generating unit commitment in one-hour intervals, just as the traditional UC model. Hence, it is shown that

it is possible to effectively incorporate ramping trajectory functions into a UC model while maintaining the same one-hour scheduling structure as before. This means that the MILP commitment structure from the traditional UC model is preserved.

Case 3 is selected to reflect some of the main challenges in future power grids: large forecasting uncertainties (in both load demand and VRES output) and steep ramping caused by a high penetration of VRES. And it is this case study that the advantages of the Bernstein UC formulation become particularly prominent. The Bernstein UC model completely dominates the traditional UC model in terms of net costs, auxiliary generation and ramping scarcity. More specifically, the robust with ES submodel performs best of all the proposed submodels. The Bernstein UC model has proven highly suitable for scheduling ES unit operation.

7.4 Future Work

This thesis has proposed a Bernstein UC formulation with the same scheduling structure as the traditional UC model, using the same input parameters and commitment variables. Simulations done on the Bernstein UC formulation has shown significant potential for reducing net operation costs, ramping scarcity and the need for auxiliary generation during RT operation. The model, however, is however based on a number of simplifications. Some possible future directions of this work are:

- An ES unit RT operation model. Running the charging/discharging cycles based on DA-scheduling may cause problems when there are large forecast errors. In certain scenarios, power system operation may be infeasible without auxiliary generation e.g. when ES units are charging in the DA schedule.
- Introducing stochastic spinning/standing reserve constraints for the entire power system, zones or buses, and functions that integrate demand response into the model.
- Improved robust optimization model. The robust UC model suggested in this model benefited the traditional UC model far more than the Bernstein model. It may be ideal to redesign a robust optimization model for optimal effect on the Bernstein UC model.
- In both the DA-market and the RT-market, it could be interesting to investigate the possibility of ramping market features[72][73], and not only a generating capacity market.
- The UC model in this thesis uses several deterministic constraints and considerations. Rewriting this model into a stochastic formulation could improve the performance and effectiveness of the model.

Bibliography

[1] Subcommittee, P. M. 1996. The ieee reliability test system - 1996. *IEEE TRANSACTIONS ON POWER SYSTEMS*, 14(3), 1010–1020.

[2] S.A. Kazarlis, A.G. 8akirtzis, e. a. 1996. A genetic algorithm solution to the unit commitment problem. *IEEE Transactions on Power Systems*, 11(1), 83–92.

[3] Masood Parvania, A. S. 2016. Unit commitment with continuous-time generation and ramping trajectory models. *IEEE TRANSACTIONS ON POWER SYSTEMS*, 31(4), 3169–3178.

[4] Ramteen Sioshansi, Richard O'Neill, e. a. 2008. Economic consequences of alternative solution methods for centralized unit commitment in day-ahead electricity markets. *IEEE Transactions on Power Systems*, 23(2), 83–92.

[5] reve. 2019. 51.3 gw of global wind energy capacity installed in 2018. https://www.evwind.es/2019/02/26/51-3-gw-of-global-wind-energy-capacity-installed-in-2018/66248. Accessed: 2019-05-22.

[6] Change, U. N. C. 2018. The paris agreement. https://unfccc.int/process-and-meetings/the-paris-agreement/the-paris-agreement. Accessed: 2019-05-22.

[7] Fahd, G. N. 1994. Unit commitment literature synopsis. *IEEE Transactions on Power Systems*, 9(1), 128–135.

[8] Padhy, N. 2004. Unit commitment-a bibliographical survey. *IEEE Transactions on Power Systems*, 19(2), 1196–1205.

[9] B. Saravanan, Siddharth Das, e. a. 2013. A solution to the unit commitment problem—a review. *Frontiers in Energy*, 7(2), 223–236.

[10] M. Carrion, J.M. Arroyo, e. a. 2006. A computationally efficient mixed-integer linear formulation for the thermal unit commitment problem. *IEEE Transactions on Power Systems*, 21(3), 1371–1378.

[11] Raymond B.Johnson, Shmuel S.Oren, e. a. 1997. Equity and efficiency of unit commitment in competitive electricity markets. *Utilities Policy*, 6(1), 9–19.

[12] Tao Li, M. S. 2007. Dynamic ramping in unit commitment. *IEEE Transactions on Power Systems*, 22(3), 1379–1381.

[13] C. Wang, S. S. 1993. Effects of ramp-rate limits on unit commitment and economic dispatch. *IEEE Transactions on Power Systems*, 8(3), 1341–1350.

[14] Antonio Frangioni, C. G. 2006. Solving nonlinear single-unit commitment problems with ramping constraints. *Operations Research*, 54(4), 767–775.

[15] L. M. Kimball, K. A. Clements, e. a. 1998. Economic dispatch with network and ramping constraints via interior point methods. *IEEE Transactions on Power Systems*, 13(1), 236–242.

[16] C. Wang, S. S. 1995. Optimal generation scheduling with ramping costs. *IEEE Transactions on Power Systems*, 10(1), 60–67.

[17] Wei Fan, Xiaohong Guan, e. a. 2002. A new method for unit commitment with ramping constraints. *Electric Power Systems Research*, 62(3), 215–224.

[18] C. Wang, S. S. 1994. Ramp-rate limits in unit commitment and economic dispatch incorporating rotor fatigue effect. *IEEE Transactions on Power Systems*, 9(3), 1539–1545.

[19] Germán Morales-España, Jesus M. Latorre, e. a. 2013. Tight and compact milp formulation of start-up and shut-down ramping in unit commitment. *IEEE Transactions on Power Systems*, 28(2), 1288–1296.

[20] Masood Parvania, Pramod P. Khargonekar, e. a. 2018. Scheduling and pricing of energy generation and storage in power systems. *IEEE TRANSACTIONS ON POWER SYSTEMS*, 33(4), 4308–4322.

[21] Jianhui Wang, Mohammad Shahidehpour, e. a. 2008. Levelised value of electricity - a systemic approach to technology valuation. *IEEE Transactions on Power Systems*, 23(3), 1319–1327.

[22] Lei Wu, Mohammad Shahidehpour, e. a. 2007. Stochastic security-constrained unit commitment. *IEEE Transactions on Power Systems*, 22(2), 800–811.

[23] NERC. 2019. Glossary of terms used in nerc reliability standards. https://www.nerc.com/files/glossary_of_terms.pdf. Accessed: 2019-06-04.

[24] Mathisen, A. R. 2018. *Capturing the Flexibility of Energy Storage Units in Power Systems*. Norwegian University of Science and Technology.

[25] E.V.Thomas, H.L.Case, e. a. 2003. Accelerated power degradation of li-ion cells. *Journal of Power Sources*, 124(1), 254–260.

[26] Shodor. 2019. Numerical differentiation. http://www.shodor.org/cserd/Resources/Algorithms/NumericalDifferentiation/. Accessed: 2019-02-20.

[27] Pipenbrinck, N. 1998. Hermite curve interpolation. https://www.cubic.org/docs/hermite.htm. Accessed: 2019-05-11.

[28] Weisstein, E. W. 2019. Bernstein polynomial. http://mathworld.wolfram.com/BernsteinPolynomial.html. Accessed: 2019-02-19.

[29] Joy, K. I. 2000. Bernstein polynomials. http://graphics.cs.ucdavis.edu/education/CAGDNotes/Bernstein-Polynomials.pdf. Accessed: 2019-06-04.

[30] ICPS. 2006. Symbolic polynomial maximization over convex sets with bernstein expansion. http://icube-icps.unistra.fr/index.php/Main_Page. Accessed: 2019-03-06.

[31] Subcommittee, P. M. 1979. Ieee reliability test system. *IEEE Transactions on Power Apparatus and Systems*, PAS-98(6), 2047–2054.

[32] ISO, C. 1998. Load data. http://www.caiso.com/Pages/default.aspx. Accessed: 2019-05-11.

[33] Soroudi, A. 2017. *Power System Optimization Modeling in GAMS*. Springer.

[34] Christos Ordoudis, Pierre Pinson, e. a. 2016. *An Updated Version of the IEEE RTS 24-Bus System for Electricity Market and Power System Operation Studies*. DTU.

[35] Aitor Makibar, Luis Narvarte, e. a. 2017. On the relation between battery size and pv power ramp rate limitation. *Solar Energy*, 142(1), 182–193.

[36] Kong Soon Ng, Chin-Sien Moo, e. a. 2009. Enhanced coulomb counting method for estimating state-of-charge and state-of-health of lithium-ion batteries. *Applied Energy*, 86(9), 1506–1511.

[37] Ahmad Nikoobakht, Jamshid Aghaei, e. a. 2019. Assessing increased flexibility of energy storage and demand response to accommodate a high penetration of renewable energy sources. *IEEE Transactions on Sustainable Energy*, 10(2), 659–669.

[38] Bram L.Gorissen, İhsan Yanıkoğlu, e. a. 2015. A practical guide to robust optimization. *Omega*, 53(1), 124–137.

[39] Alexandre Street, Fabrício Oliveira, e. a. 2011. Contingency-constrained unit commitment with n-k security criterion: A robust optimization approach. *IEEE Transactions on Power Systems*, 26(3), 1581–1590.

[40] Zukui Li, C. A. F. 2011. *ROBUST COUNTERPART OPTIMIZATION: UNCERTAINTY SETS, FORMULATIONS AND PROBABILISTIC GUARANTEES*. Department of Chemical and Biological Engineering, Princeton University.

[41] Yongpei Guan, J. W. 2013. Uncertainty sets for robust unit commitment. *IEEE Transactions on Power Systems*, 29(3), 1439–1440.

[42] Chaoyue Zhao, Yongpei Guan, e. a. 2013. Unified stochastic and robust unit commitment. *IEEE Transactions on Power Systems*, 28(3), 3353–3361.

[43] Qiaoyan Bian, Huanhai Xin, e. a. 2014. Distributionally robust solution to the reserve scheduling problem with partial information of wind power. *IEEE Transactions on Power Systems*, 30(5), 12822 – 2823.

[44] Yu An, B. Z. 2015. Exploring the modeling capacity of two-stage robust optimization: Variants of robust unit commitment model. *IEEE Transactions on Power Systems*, 30(1), 109–122.

[45] Long Zhao, B. Z. 2012. Robust unit commitment problem with demand response and wind energy. *2012 IEEE Power and Energy Society General Meeting, San Diego, CA*, 1(1), 1–8.

[46] Alireza Soroudi, Pierluigi Siano, e. a. 2016. Optimal dr and ess scheduling for distribution losses payments minimization under electricity price uncertainty. *IEEE Transactions on Smart Grid*, 7(1), 261–272.

[47] Ruiwei Jiang, J. W. 2012. Robust unit commitment with wind power and pumped storage hydro. *IEEE Transactions on Power Systems*, 27(2), 800–810.

[48] Hongxing Ye, Jianhui Wang, e. a. 2017. Mip reformulation for max-min problems in two-stage robust scuc. *IEEE Transactions on Power Systems*, 32(2), 1237–1247.

[49] Dimitris Bertsimas, Eugene Litvinov, e. a. 2013. Adaptive robust optimization for the security constrained unit commitment problem. *IEEE Transactions on Power Systems*, 28(1), 52–63.

[50] C. Zhao, J. Wang, J. e. a. 2013. Multi-stage robust unit commitment considering wind and demand response uncertainties. *IEEE Transactions on Power Systems*, 28(3), 2708–2717.

[51] Frances Brazier, Frank Cornelissen, e. a. 1998. Agents negotiating for load balancing of electricity use. https://www.cs.vu.nl/~wai/demas/loadb/icdcs_11.html. Accessed: 2019-05-14.

[52] T. Boßmann, I. S. 2015. The shape of future electricity demand: Exploring load curves in 2050s germany and britain. *Energy*, 90(2), 1317–1333.

[53] Ignacio Marti, Georges Kariniotakis, e. a. 2006. Evaluation of advanced wind power forecasting models – results of the anemos project. *European Wind Energy Conference*.

[54] Aidan Tuohy, Peter Meibom, e. a. 2019. Unit commitment for systems with significant wind penetration. *IEEE Transactions on Power Systems*, 24(2), 592–601.

[55] Hazen, G. B. 2001. Stochastic trees and the stotree modeling environment: Models and software for medical decision analysis. *Northwestern University*.

[56] Pablo A. Ruiz, C. Russ Philbrick, e. a. 2019. Wind power day-ahead uncertainty management through stochastic unit commitment policies. *2009 IEEE/PES Power Systems Conference and Exposition*.

[57] Commission, C. E. 2018. Total system electric generation. https://www.energy.ca.gov/almanac/electricity_data/total_system_power.html. Accessed: 2019-05-26.

[58] Commission, C. E. 2019. Wind energy in california. https://www.energy.ca.gov/wind/. Accessed: 2019-05-26.

[59] Statistics, C. D. G. 2019. Statistics and charts. https://www.californiadgstats.ca.gov/charts/. Accessed: 2019-05-26.

[60] Qingchun Hou, Ning Zhang, e. a. 2019. Probabilistic duck curve in high pv penetration power system: Concept, modeling, and empirical analysis in china. *Applied Energy*, 242(1), 205–215.

[61] Saad Sayeef, Simon Heslop, e. a. 2012. Characterisation of solar power variability. *Solar intermittency: Australia's clean energy challenge*, 1(1), 23–31.

[62] Local, S. E. 2019. Solar power in california. https://www.solarenergylocal.com/states/california/. Accessed: 2019-05-26.

[63] NREL. 2019. Solar maps. https://www.nrel.gov/gis/solar.html. Accessed: 2019-05-26.

[64] Commission, C. E. 2019. Visualization of seasonal variation in california wind generation. https://www.energy.ca.gov/almanac/electricity_data/3D_Visualizations/2014-2017_CF/2014-2017_CF.html. Accessed: 2019-05-26.

[65] reliawiki. 2019. Confidence bounds. http://reliawiki.org/index.php/Confidence_Bounds. Accessed: 2019-05-26.

[66] Center, N. R. 2011. Combined standard uncertainty and propagation of uncertainty. https://www.nde-ed.org/GeneralResources/Uncertainty/Combined.htm. Accessed: 2019-05-27.

[67] Yuanchao Yang, Qiaozhu Zhai, e. a. 2012. An hour-ahead scheduling problem for a system with wind resource. *2012 IEEE Power and Energy Society General Meeting*.

[68] Bruce Dunn, Haresh Kamath, e. a. 2011. Electrical energy storage for the grid: A battery of choices. *Science*, 334(6058), 928–934.

[69] Xing Luo, Jihong Wang, e. a. 2015. Overview of current development in electrical energy storage technologies and the application potential in power system operation. *Applied Energy*, 137(1), 511–536.

[70] L. Bird, M. Milligan, e. a. 2013. Integrating variable renewable energy: Challenges and solutions. https://www.osti.gov/biblio/1097911. Accessed: 2019-05-20.

[71] ISO, C. 2011. Market notice. https://www.caiso.com/Documents/RenewableForecastingReal-TimeDispatchPersistenceMarketModel/Enhancement041018.html. Accessed: 2019-05-27.

[72] Xu, L. 2014. Flexible ramping products.

[73] B.H. Bakken, A. Petterteig, e. a. 2000. Market based ancillary services for ramping. *2000 IEEE Power Engineering Society Winter Meeting. Conference Proceedings.*

Appendix A

Case 1: May 4th 2018

Stardard UC with ES units

Bernstein

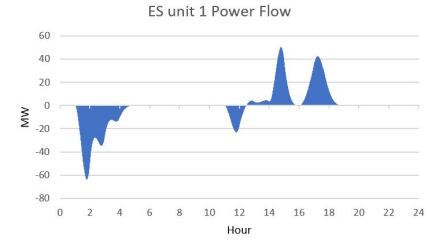

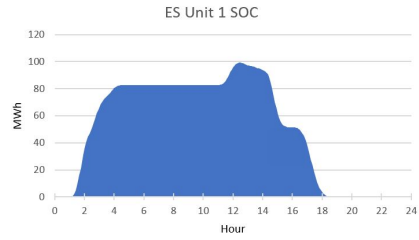

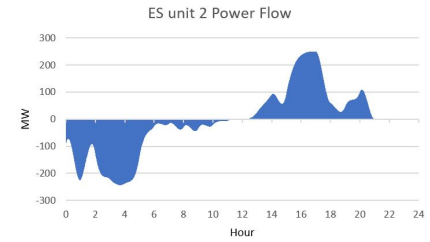

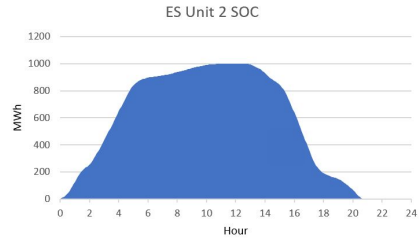

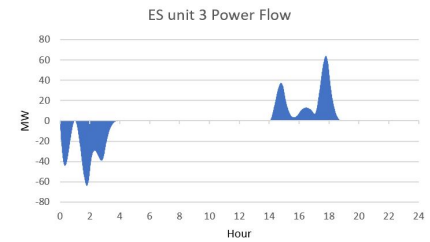

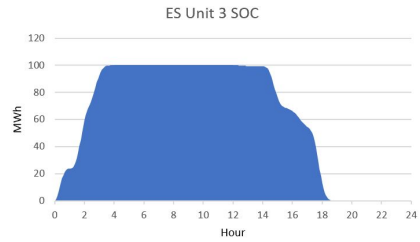

(a) ES unit power flow

(b) ES unit SOC

Traditional

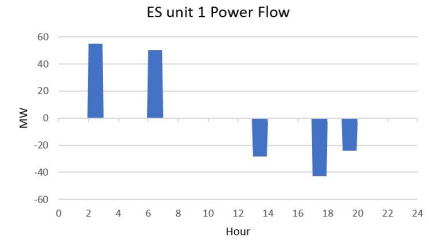

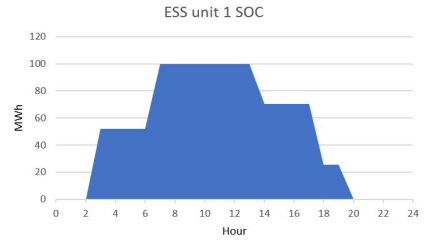

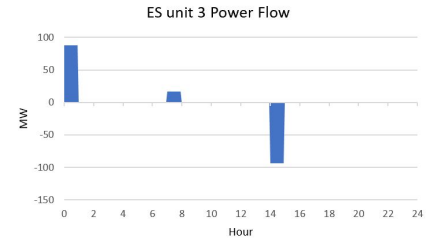

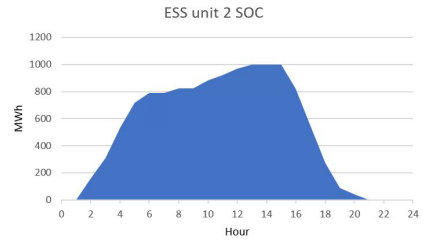

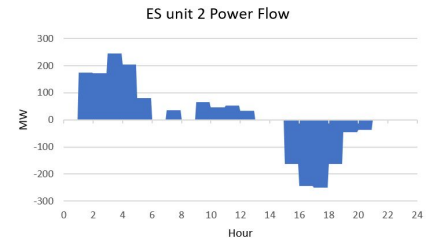

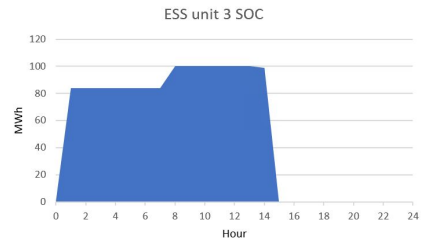

(a) ES unit power flow

(b) ES unit SOC

Robust UC with ES units

Bernstein

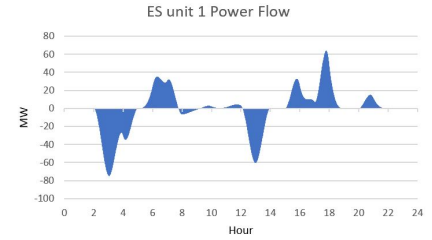

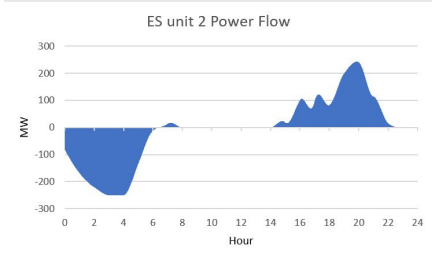

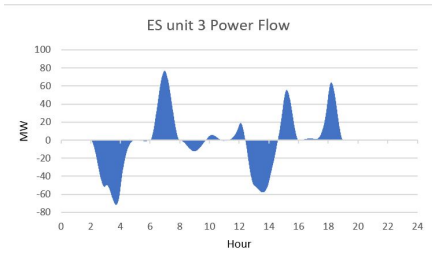

(a) ES unit power flow

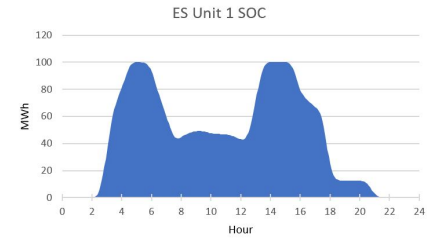

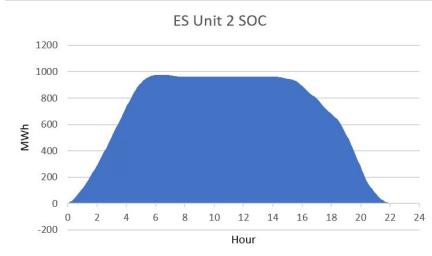

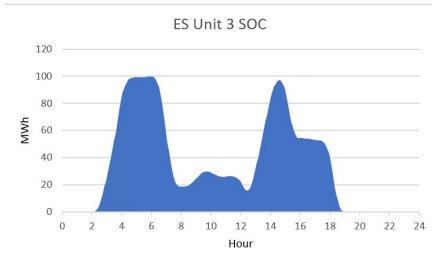

(b) ES unit SOC

Traditional

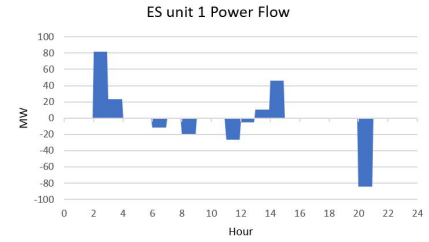

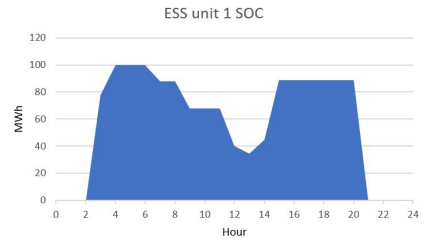

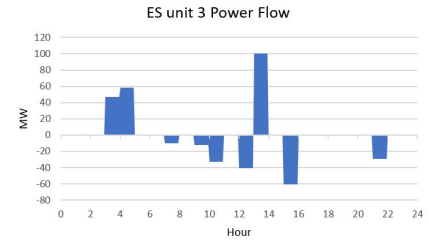

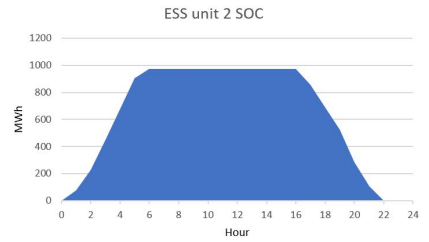

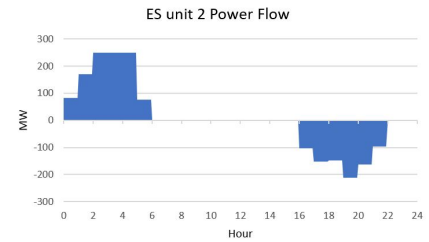

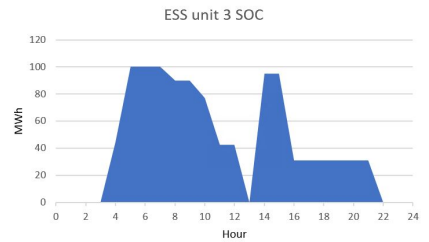

(a) ES unit power flow

(b) ES unit SOC

Case 2: August 4th 2018

Stardard UC with ES units

Bernstein

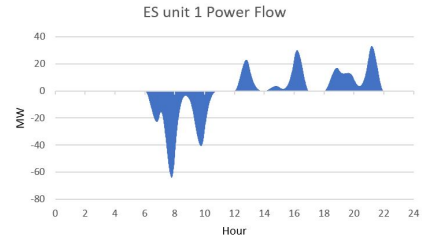

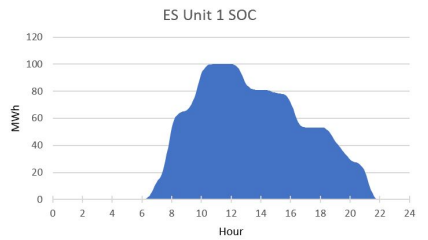

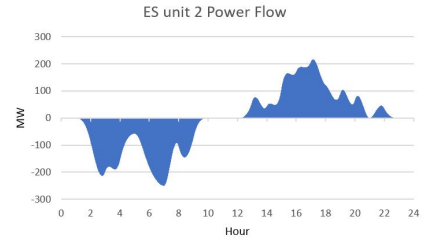

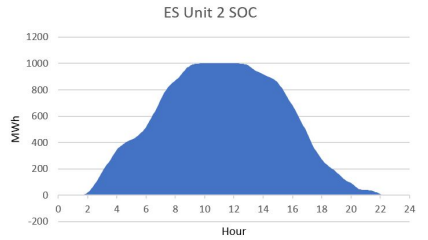

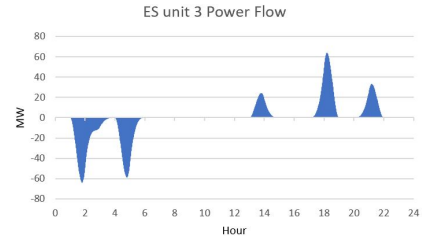

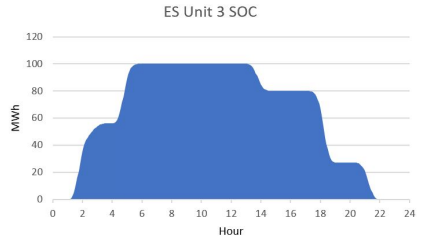

(a) ES unit power flow

(b) ES unit SOC

Traditional

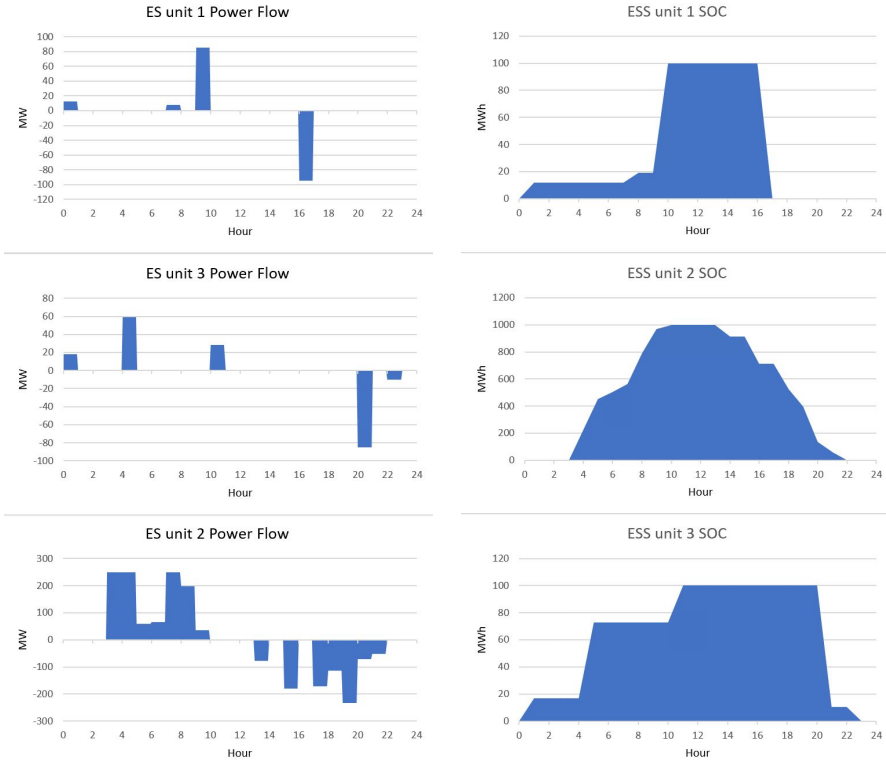

(a) ES unit power flow

(b) ES unit SOC

Robust UC with ES units

Bernstein

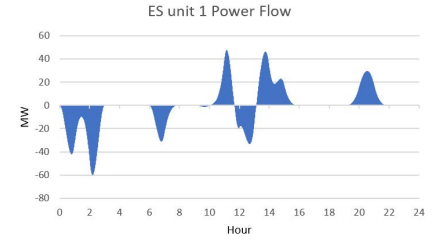

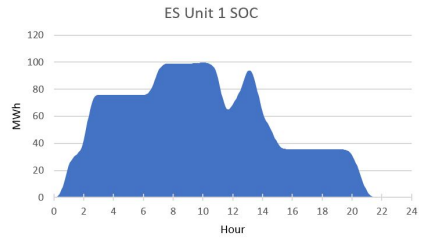

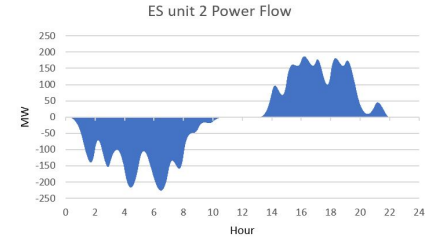

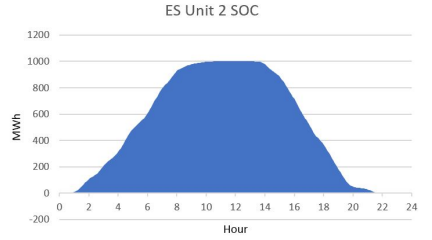

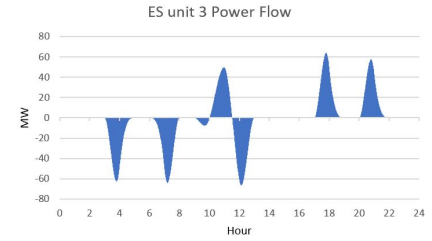

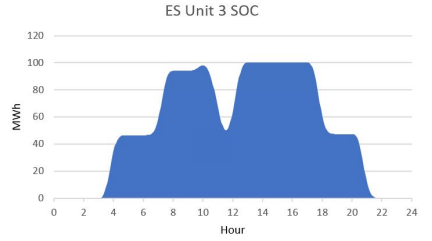

(a) ES unit power flow

(b) ES unit SOC

Traditional

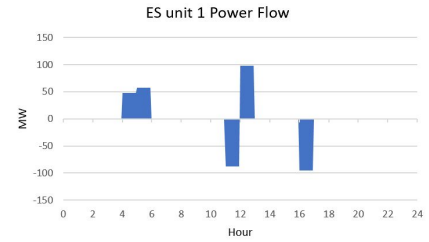

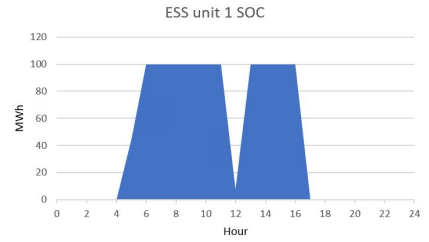

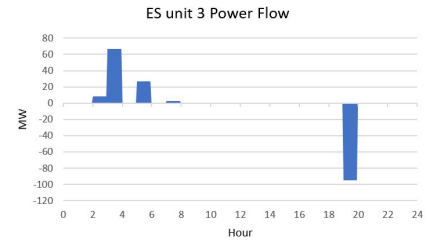

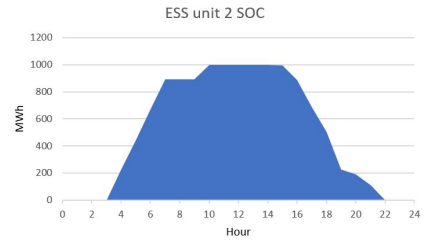

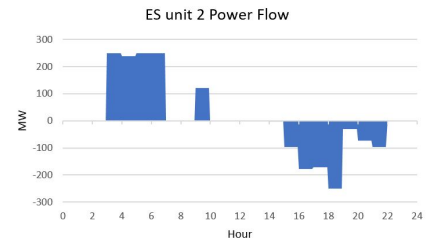

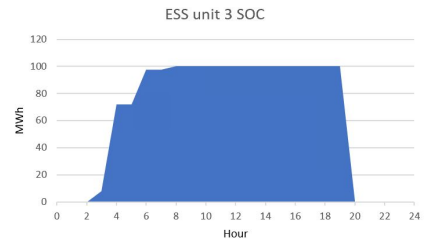

(a) ES unit power flow

(b) ES unit SOC

Case 3: July 2nd 2018

Stardard UC with ES units

Bernstein

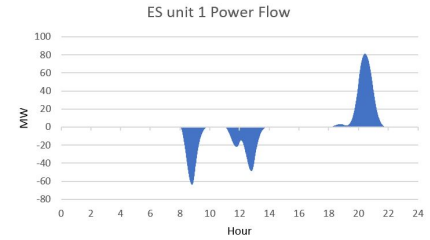

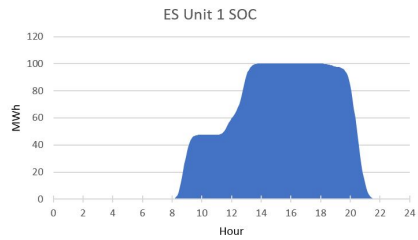

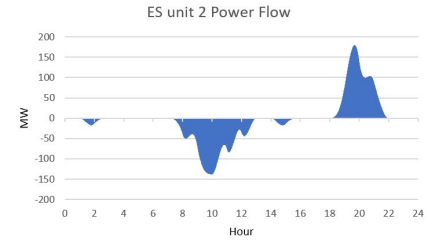

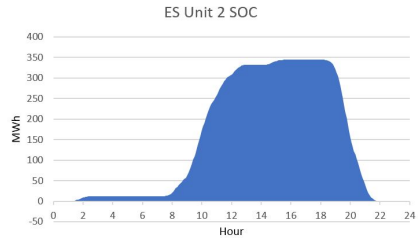

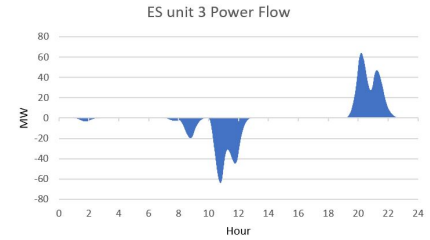

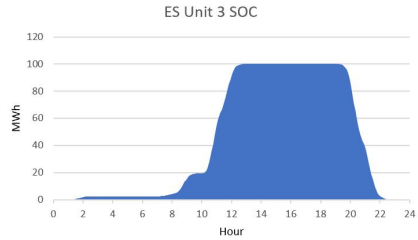

(a) ES unit power flow

(b) ES unit SOC

Traditional

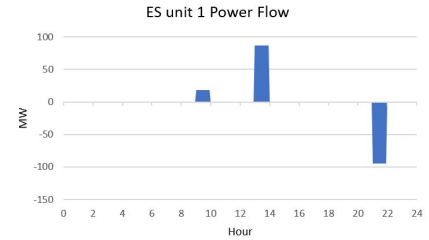

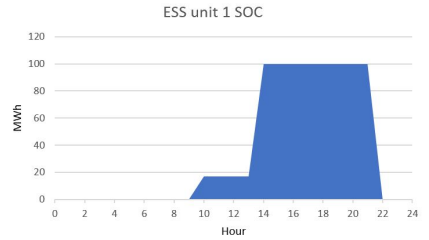

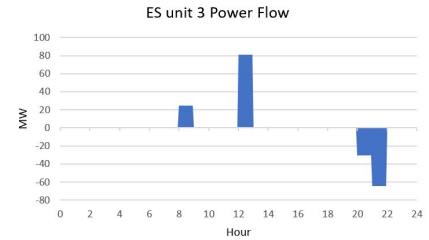

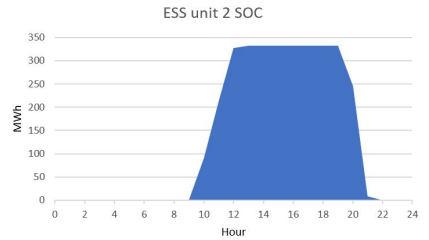

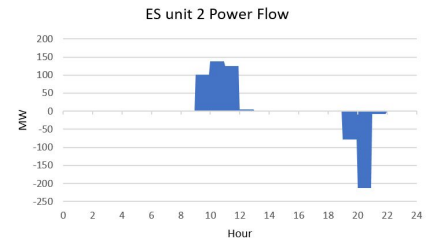

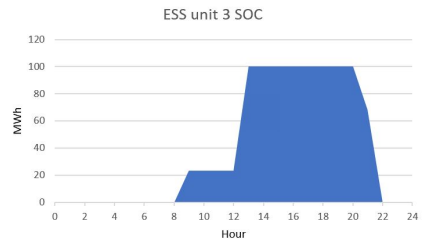

(a) ES unit power flow

(b) ES unit SOC

Robust UC with ES units

Bernstein

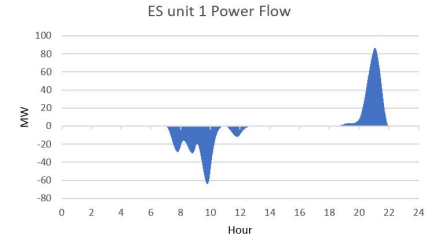

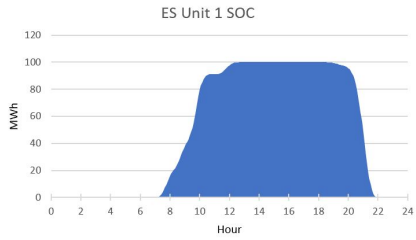

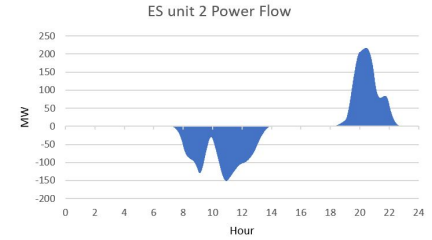

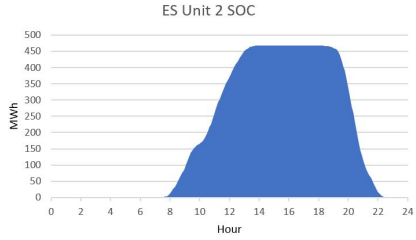

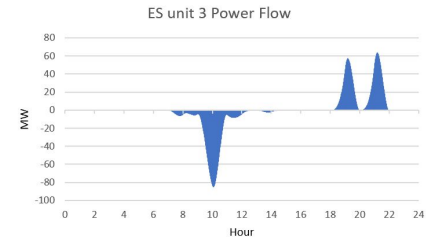

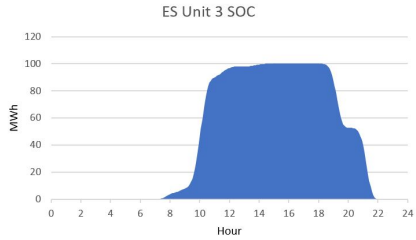

(a) ES unit power flow

(b) ES unit SOC

Traditional

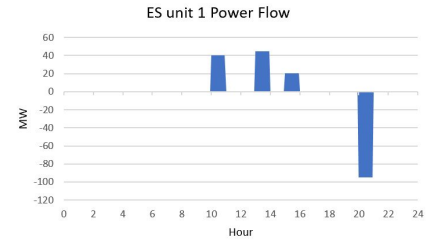

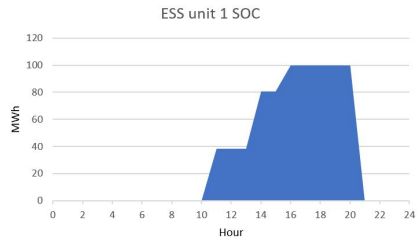

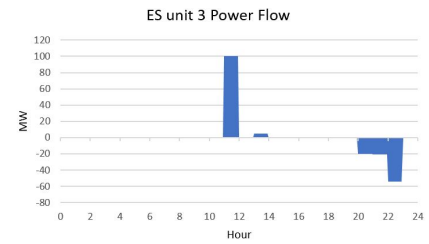

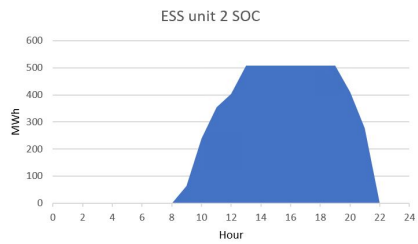

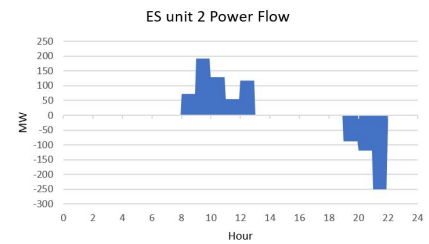

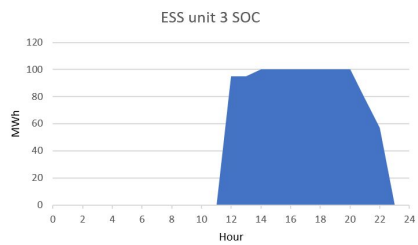

(a) ES unit power flow

(b) ES unit SOC

Appendix B

Bus	Bus Load % of System Load
1	3.8
2	3.4
3	6.3
4	2.6
5	2.5
6	4.8
7	4.4
8	6.0
9	6.1
10	6.8
13	9.3
14	6.8
15	11.1
16	3.5
18	11.7
19	6.4
20	4.5

Table 7.1: IEEE 24-bus RTS Load distribution

From Bus	To Bus	Rating (MVA)
1	2	175
1	3	175
1	5	175
2	4	175
2	6	175
3	9	175
3	24	400
4	9	175
5	10	175
6	10	175
7	8	175
8	9	175
8	10	175
9	11	400
9	12	400
10	11	400
10	12	400
11	13	500
11	14	500
12	13	500
12	23	500
13	23	500
14	16	500
15	16	500
15	21	500
15	21	500
15	24	500
16	17	500
16	19	500
17	18	500
17	22	500
18	21	500
18	21	500
19	20	500
19	20	500
20	23	500
20	23	500
21	22	500

Table 7.2: IEEE 24-bus RTS line ratings

Appendix C

GAMS Code
MATLAB Code
EXCEL Code

(RESTRICTED PUBLIC ACCESS.)